To appear in *Journal of Geophysical Research* 1996

Analysis of UARS data in the southern polar vortex in September 1992 using a chemical transport model

M.P. Chipperfield
Department of Chemistry, University of Cambridge, U.K.

M.L. Santee, L. Froidevaux, G.L. Manney, W.G. Read, J.W. Waters
Jet Propulsion Laboratory, California Institute of Technology, Pasadena, CA, U.S.A.

A.E. Roche
Lockheed Palo Alto Research Laboratory, Palo Alto, California

J.M. Russell
NASA Langley Research Center, Hampton, Virginia

Abstract

We have used a new, isentropic-coordinate three-dimensional chemical transport model to investigate the decay of ClO and evolution of other species in the Antarctic polar vortex during September 1992. The model simulations cover the same southern hemisphere period studied in a companion data paper by *Santee et al.* [this issue]. The model is initialized using the available data from the Microwave Limb Sounder (MLS) and Cryogenic Limb Array Etalon Spectrometer (CLAES) on the Upper Atmosphere Research Satellite (UARS). During the model initialization chemical inconsistencies in the UARS data became evident. Fields of *odd nitrogen* (NO_y) derived from CLAES N_2O underestimated the sum of the direct observations of the major NO_y species. Results from the model integrations at 465 K and 585 K are sampled in the same way as the various UARS instruments and *compared* to the observations both directly and by considering average quantities in the inner and edge vortex regions. Sampling the observed species in the same way as the UARS instruments is important in removing any spurious trends due, for example, to changing solar zenith angle. While the model can reproduce the magnitude of the MLS ClO observations at 585 K, this is not possible at 465 K. The model partitions too much ClO into Cl_2O_2 to reproduce the observed ClO which is around 2.0 parts per billion by volume (ppbv) averaged within the polar vortex. The model also underestimates CLAES $ClONO_2$ in the inner vortex at 465 K due to heterogeneous processing. The observations require that effectively all of the inorganic chlorine is in the form of ClO and $ClONO_2$ in the inner vortex at this altitude. In the basic model run, the decay of ClO produces $ClONO_2$ which is not observed by CLAES. Our results indicate the potential importance of the speculative reaction between OH and ClO producing HCl for the recovery of HCl in the Antarctic spring. By including this

reaction, the decay of model ClO into HCl is enhanced, yielding better agreement with HCl data from the Halogen Occultation Experiment (HALOE) data. Similar results can also be obtained by including the reaction between HO_2 and ClO to produce HCl with a 3% channel. The model generally reproduces the observed O_3 destruction during September. The most significant discrepancy for O_3 is in the inner vortex at 650 K where the model underestimates the observed O_3 loss, especially when the effects of vertical motion are included.

Introduction

In a companion paper, *Santee et al.* [this issue] (hereinafter referred to as S96) discuss the deactivation of ClO as observed by the Microwave Limb Sounder (MLS) during February 1993 in the northern hemisphere and during September 1992 in the southern hemisphere. In the northern hemisphere the observed decay of ClO was accompanied by an increase in $ClONO_2$ observed by the Cryogenic Limb Array Etalon Spectrometer (CLAES) and the chlorine budget appeared closed. However, in the southern hemisphere the decay of ClO in September was not matched by an increase in $ClONO_2$. In fact the CLAES $ClONO_2$ data showed a slight negative trend at 585 K within the polar vortex. Because of this apparent discrepancy, in this paper we study the period of September 1992 using an off-line chemical transport model initialized using Upper Atmosphere Research Satellite (UARS) data and constrained by meteorological analyses.

Off-line three-dimensional chemical transport models (CTMs) are becoming widely used in studies of stratospheric chemistry. When these models are forced by analyzed meteorological winds they provide a powerful framework for the interpretation of a wide range of stratospheric data [e.g., *Rood et al.*, 1989; *Kaye et al.*, 1990; *Lefèvre et al.*, 1994; *Chipperfield et al.*, 1994]. In this study we use a new three-dimensional CTM (SLIMCAT) which is a development of an existing CTM, TOMCAT, which is formulated on hybrid sigma/pressure levels. The main improvement of the SLIMCAT CTM over the TOMCAT CTM is the use of an isentropic vertical coordinate with a radiation scheme to calculate the vertical motion.

It is important to understand quantitatively ClO deactivation in the polar regions as this will place a limit on the rapid chlorine-catalyzed O_3 depletion. In a recent paper, *Douglass et al.* [1995] commented on the different recovery (ClO deactivation) regimes which occur in the northern and southern hemispheres. While the ClO decays into $ClONO_2$ in the northern hemisphere, this is not observed in the south. *Douglass et al.* [1995] argued that low O_3 causes the Cl concentration to increase relative to ClO permitting the faster recovery of HCl in the southern hemisphere; such possible conditions were also mentioned by *Prather and Jaffe* [1990] and *Chipperfield* [1990].

The following section describes the SLIMCAT CTM. The model experiments are then described followed by details of the chemical initialization of the model from UARS data. The results of the model simulations are then presented followed by a summary.

SLIMCAT CTM

As the CTM has not been described elsewhere, a few general details are presented here. The details of the experiments discussed in this paper are given at the end of this section. The SLIMCAT isentropic three-dimensional CTM is a development of the TOMCAT three-dimensional CTM first described by *Chipperfield et al.* [1993]. The TOMCAT CTM uses the same vertical grid as the prescribed wind and temperature fields which are either isobaric or hybrid pressure/sigma levels as used in many general circulation models (GCMs). In TOMCAT the vertical velocities are calculated by integrating the divergence of the horizontal winds. In SLIMCAT the vertical levels are surfaces of constant potential temperature (θ) which are more appropriate for stratospheric tracer transport. The horizontal wind and temperature fields are interpolated from the analysis (or GCM) levels onto the model θ levels. The SLIMCAT vertical grid is completely independent of the analyses (or GCM) levels and the vertical domain of SLIMCAT is limited by the maximum and minimum θ levels which are completely contained within the analysis (or GCM) vertical domain. The independence of the SLIMCAT vertical grid from the analysis (or GCM) grid means that the model can be run with very high vertical resolution. Alternatively, the model can be run at just a few levels in a particular region of interest permitting high horizontal resolution. The versatility of this model, the ability to use a small number of layers, is a strength. The vertical, purely diabatic, motion in the model is calculated using the MIDRAD radiation scheme [*Shine* 1987]. The thermal infrared scheme is as described by *Shine* [1987] although Curtis matrices are not used and so nonlocal thermodynamic equilibrium (non-LTE) is not accounted for. The solar scheme is that of *Shine and Rickaby* [1989]. The radiation scheme uses dummy levels above and below the SLIMCAT levels to take account of the rest of the atmosphere. The model can also be run with the vertical transport switched off, which produces unconnected isentropic levels.

The model vertical grid is defined by specifying θ at the centers and interfaces of the model levels. The horizontal winds and temperatures (obtained from

spectral coefficients in the case of ECMWF analyses used here) are interpolated from the analysis levels to the centers of the SLIMCAT isentropic levels. Temperature is also interpolated to the level interfaces, permitting the calculation of pressure at the level interfaces and therefore the mass per unit area contained in the model level. This mass thickness is used to convert the horizontal winds to horizontal mass fluxes which are then used to derive the spectral coefficients of the divergence and vorticity of the mass fluxes on isentropic levels. The use of spectral coefficients allows a straightforward change of horizontal resolution and allows the mass fluxes to be calculated at the horizontal box interfaces by choosing the correct spectral transform. For a given isentropic level the mass thickness of a level can change by a factor of 2 over the globe due to temperature variations. The model advects (and conserves exactly) total air mass as well as tracer mass and the mass content of a box after a transport step will not necessarily be equal to that derived from the analysis temperature fields. Furthermore, because the calculation of the vertical winds is independent of the specified horizontal winds the transport of total mass in the model will not necessarily balance: the decrease/increase in mass at a point in the model caused by the divergent/convergent horizontal mass fluxes will not necessarily be balanced by the vertical transport calculated by MIDRAD. Therefore, an a posteriori correction is applied to each model box at every time step to reset the mass of the box to that calculated from the isentropic density obtained from the forcing temperature field. During this readjustment the tracer mass is also adjusted in proportion to the total mass while keeping the mixing ratio constant. The magnitude of this correction has been examined for the 20 day experiments discussed below. A simple experiment was performed using a tracer of mixing ratio 1 and not correcting the mass. After 20 days the mass of the tracer was within 15% of the calculated box mass over most of the southern polar region. In the future a more physically based adjustment to the mass fluxes will be implemented.

There are a number of benefits of using isentropic levels for tracer transport in the stratosphere. As quasi-horizontal motion in the stratosphere is near isentropic, this coordinate system gives a true separation between horizontal and vertical motion. With a 'true' baric model the quasi-horizontal transport can lead to exchange of tracers between levels. As the vertical resolution of the model is likely to be fairly coarse, not only will this lead to numerical diffusion but also other species could be perturbed, especially if the tracers are chemically active. Also, a large motivation for the creation of SLIMCAT was the availability of UK Meteorological Office (UKMO) UARS analyses up to an altitude of 0.3 hPa [*Swinbank and O'Neill*, 1994]. The analyses extend much higher than other analyses available to us (e.g., European Centre for Medium Range Weather Forecasts (ECMWF) which have a top level at 10 hPa). The UKMO analyses grid the interpolated horizontal winds u and v onto UARS pressure levels. When we used them in the TOMCAT model, the vertical winds (derived from the divergence) were noisy. In SLIMCAT the use of a radiation scheme to calculate the vertical transport avoids this problem, although the representation of the vertical transport now depends on the accurate calculation of heating rates. *Weaver et al.* [1993] discussed the use of a radiation scheme to resolve some of the problems of vertical winds from assimilated data products. *Weaver et al.* [1993] found that for simulations of many months to years, use of a radiation scheme gave a better representation of the meridional circulation, compared to the analyzed vertical winds which were continually being shocked by the assimilation procedure.

SLIMCAT uses the second-order moments advection scheme of *Prather* [1986], which is the scheme used in TOMCAT. This scheme is accurate and non-diffusive and well suited to the preservation of sharp gradients that can be produced in both the horizontal and the vertical, for example, during cases of polar stratospheric cloud (PSC) processing. The model can also be used with a first-order moments advection scheme or zero order moments scheme to reduce the memory requirement.

SLIMCAT can be used simply as a transport model for passive tracers or with any idealized chemistry scheme. Alternatively, the model can be coupled with a detailed stratospheric chemistry scheme. The scheme used here is identical to that used in TOMCAT and the species considered are listed in Table 1. The chemical scheme has a treatment of heterogeneous chemistry on PSCs [*Chipperfield et al.*, 1993, 1994] and sulfate aerosols [*Chipperfield et al.*, 1995]. The occurrence of type I PSCs is predicted using the model fields of HNO_3, H_2O, and temperature and the algorithm of *Hanson and Mauersberger* [1988]. The model does not contain any microphysics or supersaturation: the PSCs occur whenever they are thermodynamically possible.

In this paper we have used the CTM to conduct experiments in the lower stratosphere for September 1992. As the region of interest is the lower stratosphere, we have used ECMWF analyses with the spectral truncation of T42 to force the model because these are available 6-hourly. In this region, diabatic heating rates are small and so most experiments were performed without vertical transport. The model horizontal resolution was that of the Gaussian grid associated with this spectral truncation (2.8°x2.8°). The model was run with three θ surfaces centered at 465 K, 585 K, and 655 K. The level at 655 K was included so that descent into the layer at 585 K could be treated correctly. Photochemical data were generally taken from *DeMore et al.* [1994]. For the absorption cross sections of Cl_2O_2 the data of *Burkholder et al.* [1990] was used in the wavelength region of 350-410 nm, which is the critical wavelength region for determining photolysis rates in the polar lower stratosphere.

Experiments

In the six experiments the model was integrated on three θ levels from 1200 UT August 31, 1992, for 20 days (32 days for runs B, D, and F). Run A was the basic model which included vertical motion. In run B, vertical motion was excluded; the three separate layers evolved independently. Experiment C was identical to experiment B except the photolysis coefficient for Cl_2O_2 was increased by a factor of 1.5. Experiment D was identical to experiment B except it included an 8% channel for reaction (R1) below. Finally, experiment E was identical to experiment B except it included a 0.3% channel for reaction (R3) below, while experiment F included a 3% channel for reaction (R3). The experiments are summarized in Table 2.

The net vertical motion produced in the model in run A was analyzed. On September 20, after 20 days integration, the net descent (change in θ) of air at 585 K was ~20 K at the center of the vortex. At 465 K the maximum descent was ~10 K at the edge of the vortex, with less descent at center (not shown). These correspond to average vertical velocities of ~0.45 mm/s at 585 K and ~0.28 mm/s at 465 K. Because the vertical motion was small, run B was taken as the standard model to simplify the interpretation of results. Based on CLAES data, S96 calculated the average vertical motion in the vortex during this period to be ~0.5±0.3 mm/s at 585 K and ~0.7±0.2 mm/s at 465 K and discussed the effect of this on ClO_x (= ClO + $2Cl_2O_2$) and $ClONO_2$.

Experiment C was performed to force the ClO:Cl_2O_2 partitioning in favor of ClO. As we have used the Cl_2O_2 cross section values of *Burkholder et al.* [1990] between 350 and 410 nm, which are larger than very recent recommendations [*DeMore et al.* 1994], experiment C is probably pushing J_{Cl2O2} above the limit of uncertainty. However, run C (discussed below), illustrates that even this increase in J_{Cl2O2} cannot sufficiently alter the partitioning in favor of ClO to reproduce quantitatively the MLS ClO observations at 465 K.

Chandra et al. [1993] and *Toumi and Bekki* [1993] (using the balloon data of *Stachnik et al.* [1992]) have shown that inclusion of the following reaction

$$\text{(R1)}\quad OH + ClO \rightarrow HCl + O_2$$

as a minor channel compared to

$$\text{(R2)}\quad OH + ClO \rightarrow HO_2 + Cl$$

improves the agreement between 2D models and observations of ClO, HCl and O_3 depletion in the upper stratosphere (see also *McElroy and Salawitch* [1989] and *Natarajan and Callis* [1991]). Further, in an idealized study, *Lary et al.* [1995b] suggested that this reaction could be important for the recovery of HCl after PSC processing. However, there is no direct chemical evidence for reaction (R1). It is the thermodynamically stable channel but involves a four-center transition state. *Atkinson et al.* [1995] suggested the branching ratio for this channel should be taken as $0.02^{+0.12}_{-0.02}$. In experiment D the effect of this reaction on the decay of lower stratospheric ClO was investigated quantitatively by comparison with UARS data. We adopted a yield of 8% for reaction (R1) similar to the previous modeling studies cited above.

Another speculative reaction which could lead to HCl formation is

$$\text{(R3)}\quad HO_2 + ClO \rightarrow HCl + O_3$$

as a minor channel compared to

$$\text{(R4)}\quad HO_2 + ClO \rightarrow O_2 + HOCl$$

Although reaction (R3) is strongly exothermic it would also require a four-centered transition state. *Burrows and Cox* [1981] measured the upper limit for the quantum yield of this channel to be 0.3%, which is the current IUPAC recommendation [*Atkinson et al.*, 1995].

Finkbeiner et al. [1995] have recently reported large values which increase with decreasing temperature. At 210 K they measured the yield for reaction (R3) to be 5±2%. The effect of this reaction was investigated in experiments E and F. Experiment E used the currently recommended upper limit of 0.3% for the quantum yield of (R3), while run F used a value of 3%.

Initialization

For short case study integrations of CTMs the chemical initialization is critically important if the simulation is to be realistic. For this study the UARS data for August 31 was interpolated onto the T42 Gaussian grid on the isentropic surfaces θ= 465 K, θ= 585 K, and θ= 655 K. The MLS O_3 data used is version 3. For H_2O, HNO_3 and ClO, data from more recent MLS retrievals are used, as described below. The CLAES data is version 7 and the Halogen Occultation Experiment (HALOE) HCl data used below for the model comparison is version 17 [*Russell et al.*, 1996]. When HNO_3 values depart substantially from climatology (e.g., following denitrification in the Antarctic polar vortex), MLS version 3 ClO values are too large by around 0.1 parts per billion by volume (ppbv) at 22 hPa and around 0.2 ppbv at 46 hPa [*Waters et al.*, 1996]. In this study we use ClO values from preliminary algorithms that also retrieve HNO_3, eliminating the bias in the version 3 data. *Waters et al.* [1995] also report a scaling error in the ClO data due to the ClO line strength factor being 8% greater than the value used in the current retrievals. We account for this by reducing the MLS ClO abundances by 8%. S96 give further details of the UARS data and details of the instrument errors. The UARS data are not entirely self-consistent and so the model initialization is not straightforward. All six experiments were initialized in the same way. In the absence of observations the CTM takes the initial chemical conditions from a 2D (latitude-height) model initialized in potential vorticity (PV) - θ space using the method of *Lary et al.* [1995a] which was based on a technique first described by *Schoeberl et al.* [1989].

The MLS and CLAES instruments on UARS make measurements on both the ascending and the descending side of the spacecraft orbit. Except during UARS yaw maneuvers, either the ascending or the descending side will correspond to mainly daytime measurements and the other side will correspond to mainly nighttime measurements. (During the yaw period both ascending and descending sides of the orbit can have significant numbers of daytime measurements). For the period studied here, the descending side corresponded to mainly daytime measurements up to September 3. After this date the ascending side made mainly daytime measurements. For short-lived species (e.g., ClO) it is important to distinguish between the ascending and the descending measurements on a given day, while for long-lived species (e.g., O_3) use of both ascending and descending sides together reduces the random errors in the data.

Long-Lived Tracers

UARS data for August 31 was used for the model initialization. CH_4 and N_2O were specified from CLAES data (averaged from the ascending and descending sides). O_3 was specified from (ascending and descending) MLS data [*Froidevaux et al.*, 1996]. H_2O was specified from the nonlinear MLS iterative retrieval [*Santee et al.*, 1995].

Odd Nitrogen Species

Observations from recent polar campaigns have shown the important role of measurements of long-lived tracers, such as N_2O, as a coordinate framework for other observations. Related to this are the correlations that are observed between pairs of long-lived tracers [*Fahey et al.*, 1990; *Plumb and Ko*, 1992]. Measurements of one long-lived tracer can therefore be used to derive other long-lived tracers. In this way the CLAES N_2O could be used to derive the expected total odd nitrogen (NO_y^* in ppbv) from the expression

$$[NO_y^*] = 20.7 - 0.0644[N_2O] \qquad (1)$$

from *Loewenstein et al.* [1993] based on Arctic data. This expression is derived from ER-2 data and has not yet been validated at altitudes above 20 km. The above correlation will not apply if there has been denitrification/sedimentation which certainly occurs in the austral polar vortex during winter. This estimated NO_y^* can be compared with the sum of the individual MLS HNO_3 and CLAES NO_2 and $ClONO_2$. Figure 1a shows the derived NO_y^* at 465 K. At high latitudes the maximum NO_y^* is around 10 ppbv. Between 60°S and 30°S there is a large region below 4 ppbv and over the southern tip of South America NO_y^* is slightly negative (-0.87 ppbv, not shown by the chosen shading), which results from very high N_2O values. Around the 60°S latitude circle the sum of UARS

HNO_3 + NO_2 + $ClONO_2$ has a maximum of about 15 pptv (Figure 2a). This is much larger than NO derived from CLAES N_2O in a region where denitrification should not have invalidated the comparison unlike at the center of the vortex when the measured NO_y underestimates NO_y^*. The estimated systematic error in this CLAES N_2O data is 20% with a precision of 8%. By using the extreme of the CLAES error limits with the extreme of the 15-20% error in the NO_y^* relationship [*Loewenstein et al.*, 1993], this discrepancy can be improved. At 585 K the maximum NO_y^* at high latitudes is around 15 pptv (Figure 1b). However, at 60°S the NO_y^* again underestimates the sum of UARS HNO_3 + NO_2 + $ClONO_2$ (Figure 2b). At this altitude, denitrification would certainly reduce NO_y (and probably at 465 K too) and so the discrepancy between NO_y^* and the sum of the UARS nitrogen species around 60°S is in the wrong sense for this to be the cause.

Because of the apparent problems (due, in part, to high N_2O values and the denitrification at the center of the vortex) the above correlation method was not used. HNO_3 was initialized directly from (ascending and descending) MLS data [*Santee et al.*, 1995]. In the polar region the model NO_y was limited to this MLS HNO_3 and the contribution from $ClONO_2$. CLAES NO_2 was not used to initialize the model poleward of 45°S (see below).

Chlorine Species

The problems encountered above for the N_2O:NO_y correlation obviously implied that the CLAES N_2O could not be used to derive the expected inorganic chlorine (Cl_y^*) [e.g. *Webster et al.*, 1993; *Woodbridge et al.*, 1995]. Indeed, this procedure was tested and the derived Cl_y underestimated the sum of CLAES $ClONO_2$ and MLS ClO in the vortex region, especially at 465 K.

The model chlorine species were therefore initialized using a combination of the Cl_y field from the 2D model and the descending (daytime) measurements of MLS ClO and CLAES $ClONO_2$ [*Morgenthaler et al.*, 1996] and limiting the maximum total mixing ratio to 3.3 ppbv. This sum was used as the total Cl_y unless the 2D model would have predicted more (for example, at the vortex edge). In the center and edge of the polar vortex, HCl was initialized to zero and any excess Cl_y after the initialization of first ClO and then $ClONO_2$ was added to ClO_x (ClO + $2Cl_2O_2$).

Aerosol Surface Area

The available aerosol surface area was specified in the model based on data from the SAGE II instrument (L. Thomason, personal communication, 1994). The initial surface area was constant with latitude and longitude and specified at 2 $\mu m^2/cm^3$ at 655 K, 5 $\mu m^2/cm^3$ at 585 K and 10 $\mu m^2/cm^3$ at 465 K. These values reflect the relatively high values that still persisted 15 months after the eruption of Mount Pinatubo. As mentioned above, the occurrence of PSCs within each grid box is predicted on the basis of the model fields of H_2O, HNO_3, and temperature.

Bromine Species

The bromine species were initialized from the 2D latitude-height model. The upper stratospheric loading of BrO_y was 20 parts per trillion by volume (pptv) and at the center of the vortex at 465 K there was about 19 pptv. The short-lived bromine species rapidly adjust to the local photochemical conditions.

Results

We present comparisons between the model and the UARS data by showing averages of the chemical species within the center and edge regions of the vortex at 465 K and 585 K. We calculated PV from the ECMWF analyses that are used to force the model. On each day the inner vortex region was defined by the limit of the -55 PVU (1 PVU = 10^{-6} $Km^2kg^{-1}s^{-1}$) contour at 465 K and the -130 PVU contour at 585 K. The vortex edge was then defined as the region between the inner vortex and the -25 PVU contour at 465 K and the -65 PVU contour at 585 K. Figure 3 shows the calculated position of the inner and edge vortex regions at 465 K and 585 K for September 5 and September 15. The inner/edge vortex-averaged values of MLS ClO and O_3 and CLAES $ClONO_2$ were obtained by calculating an area weighted mean of the measurements within these regions.

In the following plots the ClO and $ClONO_2$ averages were calculated from ascending data only while the O_3 averages were calculated using both ascending and descending data. For the HALOE HCl data the inner/edge vortex average is a simple mean of the individual sunrise profiles that fall within the defined PV contours on a given day. The model vortex averages were calculated in three ways. In the first method the average was an area-weighted value within the vortex at a fixed (1200 UT) time. Second,

for ClO and $ClONO_2$ the vortex average was also calculated by sampling the model at the same local time as the MLS and CLAES measurements throughout a 24-hour period. Third, for ClO a vortex average was also calculated from the model ClO sampled at 1200 local solar time (LST) at all points.

Self-Consistency of UARS Initial Data

During the process of initializing the model, it became clear that there were chemical inconsistencies between some of the UARS measurements. The problem with the CLAES N_2O has been mentioned above. Another example is MLS ClO and CLAES NO_2 at high southern latitudes on August 31 (not shown). There is a region of NO_2 greater than 2 ppbv near 330°E, 60°S and a large region exceeding 1 ppbv at higher latitudes. These high values of NO_2 are coincident with ClO values larger than 1 ppbv. Following initialization with these two fields the model chemistry would lead to rapid production of $ClONO_2$ (and decay of ClO). Because the observed ClO does not decay so rapidly we did not use the CLAES NO_2 within 10° latitude of the polar vortex.

Evolution of ClO, $ClONO_2$ and HCl

Vortex averaged quantities. Figure 4 shows the average model Cl_y species within the two vortex regions at 465 K and 585 K for run B (the standard model run without vertical transport). In this run the Cl_y is roughly constant at 2.8-3.0 ppbv at 465 K and 3.0-3.1 ppbv at 585 K. At both levels and in both regions, ClO_x is decreasing during the model run. The decay of ClO_x is more rapid in the edge vortex region compared to the inner vortex and more rapid at 585 K compared to 465 K. At 585 K the gradual decay of ClO_x in the inner vortex region produces an increase in $ClONO_2$ up to September 20, after which HCl recovers more rapidly. In the edge region at 585 K, ClO_x is lower than in the inner vortex and initially decays rapidly to $ClONO_2$, although after September 6, $ClONO_2$ itself decays and HCl increases. At 465 K in the inner vortex the decay in model ClO_x is initially slow. $ClONO_2$ increases slightly before September 20 but after this date both $ClONO_2$ and HCl increase more rapidly. At the vortex edge at 465 K the decay of ClO_x initially produces $ClONO_2$ with a small increase in HCl in late September.

Figure 5 shows the average MLS ClO inside the two vortex regions at 585 K and 465 K. (Note that the initial sharp increase in the MLS ClO is due to the changing LST of the measurements as the ascending observations move from nighttime to daytime). The ClO data show larger average values in the inner vortex compared to the edge region and also larger values at 465 K relative to 585 K. At 585 K the inner vortex ClO shows a distinct decline after September 3, while in the edge region the much lower average values are more constant. At 465 K in the inner vortex the maximum average ClO values are near 2.0 ppbv and the inference of a trend is more difficult, although the values do decline after September 10. In the vortex edge at 465 K the average ClO values are relatively constant around 0.6 ppbv.

Also shown in Figure 5 are ClO results from model run B sampled at the same local time as the MLS measurements. The global model ClO fields were stored every 30 minutes and for each grid box the output closest to the MLS measurement time was used. By sampling the model at the same LST as the MLS measurements the vortex averaged ClO (after September 4) is significantly higher compared to the sampling at 12 UT (Figure 4) at both 465 K and 585 K as daytime ClO values are used at all longitudes. At 585 K this 'daytime' ClO is very similar in magnitude to ClO_x (Figure 4) while at 465 K the 'daytime' ClO is significantly less than ClO_x (especially in the inner vortex) due to the contribution of Cl_2O_2. The decay of model ClO at 585 K in Figure 5 agrees very well with the MLS data in terms of both magnitude and trend in the inner vortex and slightly overestimates the magnitude in the vortex edge region. However, at 465 K the model underestimates the MLS observations by more than 0.5 ppbv in the inner vortex (Figure 5d). Interestingly, the decay of the model ClO at 465 K in Figure 5d (or indeed the ClO in Figure 4d) is not as strong as the decay in ClO_x. As ClO_x decreases, the partitioning between ClO and Cl_2O_2 shifts in favor of ClO thereby reducing the apparent decrease.

There may be also an influence on the observed ClO trend due to the changing LST of the MLS observations. The sharp increase in ClO before September 3 is due to the shift of the ascending observations from nighttime to daytime. S96 show that the solar zenith angle of the ascending ClO measurements then decreases from around 88° at high latitudes on September 3 to around 75° on September 17. Figures 5c and 5d also show the vortex averaged ClO from the model run B at 465 K when it is sampled at 12 LST at all longitudes. This sampling will maximize the model ClO (and minimize Cl_2O_2) for a certain amount of ClO_x and illustrate the effect of the changing LST of

MLS observations on the apparent ClO trend. This sampling results in a significant increase in the model ClO in early September (when the ascending MLS observations were still in darkness) but very similar values later in the month when the MLS measurements were essentially very close to local noon. In the inner vortex the ClO sampled at 12 LST shows very little change (although ClO_x in Figure 4 does decay slightly). At the vortex edge the ClO sampled at 12 LST dots show a more distinct downward trend than ClO sampled like MLS, which implies that the changing MLS observation times disguises the ClO trend slightly.

Figure 6 shows the average $ClONO_2$ from CLAES for the two vortex regions. At 585 K the CLAES data does not show a clear trend in the inner vortex with the average values remaining near 1.5 ppbv. In the edge region the CLAES observations appear to show a downward trend from around 1.7 ppbv on August 31 to 1.4 ppbv on September 17. At 465 K the CLAES vortex edge average remains around 1.1 ppbv with no significant trend while inside the vortex the average $ClONO_2$ increases slightly from 0.5 to 0.7 ppbv. In the single Vortex-fivcr':lr,c analysis of S96 the CLAES data showed a slight negative trend at 585 K and also at 465 K when the effects of vertical motion were accounted for.

Also shown in Figure 6 are model results from run B. At 585 K the model was sampled at both 12 UT and at the same LST as the CLAES observations. The difference between these 2 sampling patterns is around 0.1 ppbv in the inner vortex and 0.2 ppbv in the edge vortex and illustrates the effect of the $ClONO_2$ diurnal cycle. At 465 K this effect is negligible due to the slower photolysis at this altitude. At 585 K the model (sampled like CLAES) produces a significant increase in $ClONO_2$ in the inner vortex from 1.3 ppbv to 1.9 ppbv, which is not seen in the CLAES observations. In the vortex edge the model dots show a decay from September 6 but the model values are about 0.4 ppbv larger than CLAES. At 465 K at the vortex edge the model $ClONO_2$ in run B increases from around 1.0 ppbv on September 1 to 1.5 ppbv on September 17, an increase which again is not seen in the CLAES data. In the inner vortex at 465 K run B shows a slight increasing trend as the model has much lower values than CLAES in this region which is still highly activated in the model.

Generally, a number of features of run B show poor comparison with the data. The model underestimates ClO at 465 K compared to MLS data and overestimates the recovery into $ClONO_2$ compared to CLAES at 585 K and in the vortex edge at 465 K. Conversely, the model underestimates $ClONO_2$ in the inner vortex at 465 K. These discrepancies were investigated in a range of sensitivity studies which are now discussed.

In run C, where the photolysis rate of Cl_2O_2 was increased by a factor of 1.5, the results at 585 K are very similar to run B and are not shown. Figures 5c and 5d (above) include the average ClO from run C at 465 K. Increasing J_{Cl2O2} has shifted the Cl_2O_2:ClO equilibrium towards ClO and run C has around 0.2 ppbv more ClO in the inner vortex compared to run B. The increase in ClO between run C and run B in the vortex edge (where ClO_x is lower) is much less. Despite this large 50% increase to J_{Cl2O2} the model still underestimates the MLS ClO by up to 0.5 ppbv around September 10, which confirms the difficulties in quantitatively reproducing the observed values in the very low stratosphere.

By including the 8% channel for reaction (R1) in run D the results are significantly modified at both 465 K and 585 K. Figure 7 is a similar plot to Figure 4 but for run D. Although reaction (R1) is a sink of ClO the effect of this reaction depends on whether any further heterogeneous processing occurs. At 465 K compared to run B there is much more ClO_x, less $ClONO_2$, less HOCl and more HCl in run D. At this altitude there is ongoing PSC processing in the model runs. In run B the further ClO_x activation was limited by the low HCl abundance. In run D reaction (R1) forms HCl which can then be reprocessed by reaction with $ClONO_2$ to produce more ClO_x. At 585 K ClO_x in run D is similar to run B but there is less $ClONO_2$, more HCl and slightly less HOCl. At this altitude there is no further PSC processing and reaction (R1) favors the recovery of ClO_x into HCl rather than $ClONO_2$.

Results from run D are also compared with the MLS ClO and CLAES $ClONO_2$ data above (Figures 5 and 6). Compared to run B the reduced trend in $ClONO_2$ at 465 K at the vortex edge in run D is in better agreement with the CLAES data (see Figure 6 above), although the model average in the inner vortex at 465 K now underestimates CLAES by about 0.6 ppbv. At 585 K results from run D (sampled at the same time as CLAES) are in better agreement with the observed magnitude and lack of trend in the inner vortex, although the model still shows a slight increase. In the vortex edge at 585 K run D also overestimates the CLAES data, but the discrepancy is less than run B. The evolution of ClO at 585 K in

run D is similar to run B both inside and at the edge of the vortex and shows equally good agreement with the MLS ClO data (Figure 5). At 465 K, due to the ongoing processing discussed above, run D has higher average ClO than run B.

Due to its sampling pattern, HALOE did not observe the southern vortex edge region until September 17, and the inner vortex was first sampled on September 23. The vortex-averaged HALOE HCl from September 17 onwards (see also S96 Figure 10) is included in Figure 7. At 585 K in the vortex edge region the HCl increases from around 1.2 ppbv on September 17 to 1.5 ppbv. In the inner vortex at 585 K HCl is around 0.9 ppbv on September 23 which increases to 1.5 ppbv. At 465 K the HCl increases strongly in the edge region from around 0.4 ppbv on September 17 to 1.0 ppbv on October 2 and the increase in the inner vortex is similar. It is important to determine whether this apparent increase in HCl is a true temporal increase or caused by the poleward progression of the HALOE observations. At 585 K the recovery of the model vortex HCl in run D is steady from early September through to early October in both vortex regions and the model slightly underestimates the HALOE data. At 465 K the model recovery is initially slow. The rate of recovery increases slightly after September 16 and then increases more strongly after September 24. This temporal behavior in the averaged quantities agrees well with the HALOE data in the edge region but appears to overestimate HALOE in the vortex center. The increase in model HCl is obviously a true temporal increase and the agreement with HALOE suggests that this data also shows a real temporal change in HCl.

Run E contained reaction (R3) as a 0.003% channel. The recovery of HCl (and evolution of other chlorine species) was only very slightly different to run B and the results are not shown here. Figure 8 shows the average Cl_y species from run F with the 3% channel for reaction (R3). In this run the effect of this 3% channel is similar to the effect of reaction (R1) in run D.

Synoptic maps. While the above analysis has been concerned with vortex-averaged quantities, synoptic maps of chemical species from the model can also be compared with the observations. The model/data discrepancies can then be investigated in terms of structure in the chemical fields in and around the polar vortex. As model run D gave the better agreement for the vortex-averaged quantities results from this run are used. However, for comparison with the HALOE data a synoptic map on a given day is not appropriate and so the model was sampled at the same location and time as the HALOE observations over the duration of the experiment. Figure 9 shows the HALOE measurements of HCl interpolated to 465 K and 585 K for the period in late September and early October 1992. The map consists of around 15 observations per day with the lowest latitude ones corresponding to September 12 and the highest latitude ones October 5. Figure 9 also shows HCl from model run D sampled in the same way as the HALOE observations (up to October 2). At 585 K the magnitude of the model HCl at midlatitudes is similar to HALOE with values around 0.9 ppbv. The increase in HCl at the highest latitudes is slightly underestimated in the model, which may be due, in part, to the initial assumption of zero HCl in the vortex on August 31. At 465 K model run D overestimates HCl at midlatitudes. Both run D and HALOE show a relative minimum of HCl near 60°S followed by large values inside the vortex (note that the HALOE data extends further south than the model plot). Although the model vortex-averaged HCl (Figure 7) overestimates the simple HALOE HCl inner vortex average a point-by-point comparison shows that the model underestimates HALOE around 70°S. The higher model vortex average is caused by recovery of HCl nearer the pole which is then not reprocessed due to the absence of $ClONO_2$; near the vortex edge HCl can be reprocessed heterogeneously through reaction with $ClONO_2$ in the collar region.

The divergence between the average $ClONO_2$ from the model and CLAES is illustrated by considering synoptic maps of this species. At 465 K the model average $ClONO_2$ is significantly lower than CLAES in the inner vortex but similar in magnitude in the vortex edge (Figures 6c and 6d above). Figure 10b shows that at 465 K on September 5 CLAES measures over 0.25 ppbv $ClONO_2$ throughout the inner vortex (and in some areas over 0.5 ppbv) while the model has processed this air heterogeneously resulting in very low mixing ratios in this region. By September 15 (Figure 10d) the model $ClONO_2$ has increased only slightly in the collar region and is still very low in the inner vortex. On September 15 the CLAES observations again show a broader collar region than the model with 0.25 - 0.75 ppbv $ClONO_2$ in the inner vortex. Inspection of the model results show that at 465 K the model predicted a large area of type I PSCs in the vortex in early September. The area of PSCs decayed steadily but was still significant on Septem-

ber 23. PSC activity finally ceased in late September, except for a small event in early October. Figure 3d of S96 shows the aerosol extinction from CLAES '1 hi data shows PSCs were present in early September at 465 K but not later in the month. The model prediction of PSCs based on an equilibrium calculation (and analyzed temperatures) appears to 01,,,,,,,,,, PSC activity at this altitude. The low $ClONO_2$ the model inner vortex is a result of heterogeneous processing early in the run and the long time scale for $ClONO_2$ recovery in the high latitude, denitrified lower stratosphere.

At 585 K the vortex averaged $ClONO_2$ from run D shows an increasing trend in the inner vortex, where the CLAES data shows no trend, and significantly overestimates the CLAES data at the vortex edge (Figures 6a and 6b above). These differences are clear in the synoptic maps. At 585 K on September 5 the model shows a continuous collar region with low values at the center (Figure 10a). The CLAES data shows higher values in the vortex with a limited collar region. By September 15 (Figure 10c) the data from CLAES still shows the same features as September 5 (the edge vortex average has decreased slightly) while in run D $ClONO_2$ has decreased in the collar region but increased in the inner vortex. At 585 K the model only predicts type I PSCs from September 1 until September 3. On all these days the PSC region is small and located over the Palmer peninsula which is interesting in terms of the apparently anomalous CLAES data in this region during this time.

Figure 11 shows a comparison between the HIRDLS ClO fields from run 1) and the MLS data. The region of high ClO is generally well reproduced in the model at both altitudes. At 585 K the area of high ClO at the edge of the vortex is too large in the model run the magnitude of the highest ClO observed by MLS on September 5 is well reproduced. The decay of ClO at 585 K in the model is slightly too slow. At 465 K, Figures 11b and 11d again emphasize that the model cannot reproduce the maximum observed values of ClO. In the run D the maximum model values are around 1.8 ppbv inside the vortex, while 11, MLS values are over 2.25 ppbv in certain regions of the vortex.

Ozone Loss

Figure 12 shows the average O_3 from experiments A, B, C and D along with the MLS data at the center and edge of the polar vortex at 465 K and 585 K. The MLS data shows the fastest rate of O_3 depletion in the inner vortex at 465 K (around 60 ppbv/day), and a slightly slower rate in the edge region at this altitude. At 585 K the inner vortex ozone loss rate is significantly slower than the same region at 465 K. The MLS data shows that we are considering a period during which O_3 loss is ongoing but before very low (near zero) O_3 mixing ratios occur. At the edge of the vortex all 4 experiments show similar loss rates which fit the data well at 465 K and slightly overestimate the loss at 585 K. In the inner vortex region model run B underestimates the depletion at 465 K and overestimates the depletion at 585 K. By including the effects of vertical motion (run A) the agreement is therefore better at 585 K but worse at 465 K following the descent of higher O_3 mixing ratio air. Compared to run B, run C gives a larger ozone depletion at 465 K (in better agreement with the observations) and very similar results at 585 K where the Cl_2O_2 cycle is less important for destroying ozone. Compared to run B, run D produces a stronger depletion at 465 K (due to higher ClO_x), again in better agreement with the observations, and slightly less depletion than run B at 585 K (due to faster deactivation). The underestimation of the observed O_3 loss in the inner vortex at 465 K is important as this is the region where there was the largest discrepancy between the model and observed ClO. If the model had higher ClO values in this region, similar to those measured by MLS, the modeled ozone loss would be larger.

Summary

We have used a new three-dimensional chemical transport model to study the evolution of chlorine species (and ozone) in the Antarctic polar vortex during September 1992. The model uses an isentropic vertical coordinate and the horizontal winds are specified from meteorological analyses or GCM output. Vertical advection is calculated using the MIDRAD stratospheric radiation scheme. The model uses the accurate, non-diffusive transport scheme of *Prather* [1986] and can be coupled with a detailed stratospheric chemistry scheme.

This modeling study complements a companion data paper by Santee et al. [this issue] which investigated the deactivation of chlorine in the two polar regions using UARS data. The model was initialized using observations from the UARS MLS and CLAES instruments and the evolution of the model was compared with the data.

There were obvious chemical inconsistencies be-

tween some of the UARS measurements. Fields of NO_y^* and Cl_y^* derived from CLAES N_2O underestimated the sum of individual members of these families. For this reason the powerful method of tracer correlation could not be used to derive these fields in the initialization procedure.

To compare the ClO fields between the model and measurements the model was sampled at the same local time as the MLS observations. This was also necessary for the comparison of $ClONO_2$ at 585 K because at this altitude $ClONO_2$ has a detectable diurnal cycle. By sampling the model ClO like MLS certain observed trends in the ClO data can be ascribed to changing local solar times of the observations during early September.

A significant discrepancy between all of the model runs and the observations occurred for ClO at 465 K. At 585 K the model could reproduce the magnitude of the MLS observations but at 465 K the model ClO strongly underestimated MLS ClO. The MLS ClO observations approach 2.4 ppbv in localized regions of the vortex and the inner vortex average at 465 K maximizes at 2.0 ppbv. At 465 K the MLS data compare in magnitude to the model ClO_x ($ClO + 2Cl_2O_2$) but the model partitions a considerable fraction of ClO_x into Cl_2O_2. A sensitivity run was performed (run C) in which the photolysis rate of Cl_2O_2 was increased by 50% to force the $ClO:Cl_2O_2$ partioning in favor of ClO at lower altitudes. However, this large increase in J_{Cl2O2} could not force the model to reproduce the large ClO mixing ratios observed by MLS.

Another major discrepancy between the model and data occurred for $ClONO_2$. At 465 K, due to ongoing heterogeneous processing and slow ClO recovery, there is very little $ClONO_2$ in the model inner vortex. In contrast the CLAES data indicates values around 0.5 ppbv. Together with the ClO comparison mentioned above a major problem in the model is the simultaneous underestimation of both the CLAES $ClONO_2$ and MLS ClO in the inner vortex at 465 K. By simply adding these two observed quantities (e.g. Santee et al. [this issue], Figure 11) it can be seen that there is around 2.7 ppbv of chlorine tied up in these two species alone. As the model only has 3.0 ppbv of Cl_y inside the vortex at 465 K it would be impossible to reproduce both the observed ClO and $ClONO_2$, after allowance is made for Cl_2O_2.

The decay of ClO was studied in the basic model experiment and a number of sensitivity studies. In the basic model experiment (run B) ClO decays primarily into $ClONO_2$ at 465 K and in the inner vortex at 585 K which is not supported by the CLAES data. By including the reaction $OH + ClO \rightarrow HCl + O_2$ (R1) in run D the increase in $ClONO_2$ was suppressed and ClO_x decayed into HCl. The recovery of HCl in run D was therefore in better agreement with the HALOE HCl data which indicated mixing ratios around 1.5 ppbv in the vortex in late September. We also studied the reaction $HO_2 + ClO \rightarrow HCl + O_3$ (R3) in runs E and F. With a 0.3% channel the effect of this reaction in our experiments was negligible, but with a 3% channel the reaction increased recovery into HCl in a similar way to (R1).

The better agreement of run D with the HCl observations would support previous evidence [*Toumi et al.*, 1993; *Chandra et al.*, 1993] that reaction (R1) may occur with around an 8% channel. Uncertainties in the model initialization (especially of HCl) and UARS data preclude a more definite conclusion. Furthermore, the inclusion of speculative reaction (R3) with a 3% channel produced a similar effect on HCl recovery. Recent measurements [*Finkbeiner et al.*, 1995] indicating a 5% yield for this channel would imply a very important role for reaction (R3) in the stratosphere.

Compared to MLS ozone the largest discrepancy in the depletion rate occurred in the inner vortex at 465 K. This was especially true when the effects of vertical motion were included. This underestimation of the O_3 depletion in this region is interesting in relation to the disagreements between the ClO and $ClONO_2$ fields discussed above. In the outer vortex at 465 K and at 585 K the model depletion rate was generally in good agreement with the MLS data.

The numerical model experiments presented here have aided the interpretation of the UARS data presented by *Santee et al.* [this issue]. Models are able to quantify the sampling effects of diurnally varying species and test for the chemical self-consistency of different datasets. The comparison between model and data show some quantitative discrepancies. To further investigate these will require more constraint by improved UARS retrievals leading to better model initialization.

Acknowledgments. MPC thanks P. Simon of Météo France for help with the transport model, R. S. Stone and I. J. Thurburn for supplying the MIDRAD radiation scheme, J. A. Pyle for helpful comments and R. Berrisford for his assistance in obtaining the ECMWF analyses. We acknowledge use of the ECMWF analyses. The modeling work at Cambridge University

forms part of the UK Universities' Global Atmospheric Modelling Programme and is also supported by the U.K. Department of the Environment

References

Atkinson, R., D.L. Baulch, R.A. Cox, R.F. Hampson, J.A. Kerr, and J. Troe, Evaluated kinetic and photochemical data for atmospheric chemistry, Supplement V - IUPAC Subcommittee on Gas Kinetic Data Evaluation for Atmospheric Chemistry *J. Phys. Chem. Ref. Data*, (in press), 1995.

urkholder, J.B., J.J. Orlando, and C.J. Howard Ultraviolet absorption cross sections of Cl_2O_2 between 210 and 410nm, *J. Phys. Chem.*, 94, 687-695 1990.

urrows, J.P., and R.A. Cox, Kinetics of chlorine oxide radical reactions using modulated photolysis Part 4. The Reactions of Cl + Cl_2O - > Cl_2 + ClO and ClO + HO_2 - > products studied at 1 atm and 300 K, *J. Chem. Soc. Faraday Trans.*, *77*, 2455 1981.

Chandra, S., Jackman, C. H., Douglass, A. R., Fleming, E. L., Considine, D. B., Chlorine catalyzed destruction of ozone - implications for ozone variability in the upper-stratosphere, *Geophys. Res. Lett.* *20*, 351-354, 1993.

Chipperfield, M.P, J. A. Pyle, C. E. Blom, N. Glatthor, M. Höpfner, T. Gulde, Ch. Piesch and P. Simon, The Variability of $ClONO_2$ in the Arctic Polar Vortex: Comparison of Transall MIPAS Measurements and 3D Model Results, *J. Geophys. Res.*, in press, 1995.

Chipperfield, M.P., A numerical study of trace gases in the polar stratosphere, PhD Thesis, University of Cambridge, 1990.

Chipperfield, M.P., D. Cariolle, P. Simon, R. Ramaroson and D.J. Lary, A three-dimensional modeling study of trace species in the Arctic lower stratosphere during winter 1989-90, *J. Geophys. Res.* *98*, 7199-7218, 1993.

Chipperfield, M.P., D. Cariolle and P. Simon, A 3-D chemical transport model study of chlorine activation during EASOE, *Geophys. Res. Lett.*, *21*, 1467-1470, 1994.

DeMore, W.B., et al., Chemical kinetics and photochemical data for use in stratospheric modeling, JPL Publication 94-26, 1994.

Douglass, A.R., M.R. Schoeberl, R.S. Stolarski, J.W. Waters, J.M. Russell, A.E. Roche and S.T. Massie, Interhemispheric differences in springtime production of HCl and $ClONO_2$ in the polar vortices, *J. Geophys. Res.*, *100*, 13,967-13,978, 1995.

ahey, D.W., S. Solomon, S.R. Kawa, M. Loewenstein, J.R. Podolske, S.E. Strahan and K.R. Chan, A diagnostic for denitrification in the winter polar stratospheres, *Nature*, *345*, 698-702, 1990.

Finkbeiner, M., J.N. Crowley, O. Horie, R. Muller, G.K. Moortgat and P.J. Crutzen, Reaction between HO_2 and ClO: Product formation between 210 and 300 K, *J. Phys. Chem.*, *99*, 16264-16275, 1995.

Froidevaux, L., et al., Validation of UARS MLS O_3 Measurements, *J. Geophys. Res.*, (in press), 1995.

Hanson, D., and K. Mauersberger, Laboratory studies of the nitric acid trihydrate: Implications for the south polar stratosphere, *Geophys. Res. Lett.*, *15*, 855-858, 1988.

Kaye, J.A., et al., Three dimensional simulation of hydrogen chloride and hydrogen fluoride during the Airborne Arctic Stratospheric Expedition, *Geophys. Res. Lett.*, 17, 529-532, 1990.

Lary, D.J., M.P. Chipperfield, J.A. Pyle, W.A. Norton and L.P. Riishojgaard, Three-dimensional tracer initialization and general diagnostics using equivalent PV latitude - potential temperature coordinates, *Q. J. R. Meteorol. Soc.*, *121*, 187-210, 1995a.

Lary, D.J., M.P. Chipperfield, and R. Toumi, The potential impact of the reaction OH+ClO- >HCl+O_2 on polar ozone photochemistry, *J. Atmos. Chem.*, *21*, 61-79, 1995b.

Lefevre, F., G.P. Brasseur, I. Folkins, A.K. Smith and P. Simon, Chemistry of the 1991-1992 stratospheric winter: Three dimensional model simulations, *J. Geophys. Res.*, *99*, 8183-8195, 1994.

Loewenstein, M., et al., New observations of the NO_y/N_2O correlation in the lower stratosphere, *Geophys. Res. Lett.*, *20*, 2531-2534, 1993.

McElroy, M.B., and R.J. Salawitch, Changing composition of the global stratosphere, *Science, 243*, 763-770, 1990.

Mergenthaler, J.L., et al., Validation of CLAES $ClONO_2$ measurements, *J. Geophys. Res.*, (in press), 1995.

Natarajan, M., and L.B. Callis, Stratospheric photochemical studies with Atmospheric Trace Molecule (ATMOS) measurements, *J. Geophys. Res.*, *95*, 9361-9370, 1990.

Plumb, R.A., and M.K.W. Ko, Interrelationships between mixing ratios of long-lived stratospheric constituents, *J. Geophys. Res.*, *97*, 10,145-10,156 1992.

Prather, M.J., Numerical advection by conservation of second order moments, *J. Geophys. Res.*, *91* 6671-6681, 1986.

Prather, M.J., and A.H. Jaffe, Global impact of the Antarctic ozone hole: chemical propagation, *J. Geophys. Res.*, *95*, 3473-3492, 1990.

Roche, A.E., et al., Validation of CH_4 and N_2O measurements by the CLAES instrument on UARS *J. Geophys. Res.*, (in press) 1995.

Rood, R.B., D.J. Allen, W.E. Baker, D.J. Lamich and J.A. Kaye, The use of assimilated stratospheric data in constituent transport calculations, *J. Atmos. Sci.*, *46*, 687-701, 1989.

Russell, J.M., et al., Validation of hydrogen chloride measurements made by HALOE from the UARS platform, *J. Geophys. Res.*, (in press) 1995.

Santee, M.L., et al., Chlorine deactivation in the lower stratospheric polar regions during late winter: results from UARS, *J. Geophys. Res.*, (submitted) 1996.

Santee, M.L., W.G. Read, J.W. Waters, L. Froidevaux, G.L. Manney, D.A. Flower, R.F. Jarnot, R.S. Harwood and G.E. Peckham, Interhemispheric differences in polar stratospheric HNO_3, H_2O, CO and O_3, *Science*, *267*, 849-852, 1995.

Schoeberl, M.R., et al., Reconstruction of the constituent distribution and trends in the Antarctic polar vortex from ER-2 flight observations. *J. Geophys. Res.*, *94*, 16,815-16,845, 1989.

Shine, K.P., The middle atmosphere in the absence of dynamical heat fluxes, *Q. J. Roy. Meteorol. Soc.*, *113*, 603-633, 1987.

Shine, K.P., and J.A. Rikaby, Solar radiative heating due to absorption by ozone, 597-600, Proceedings of Quadrennial Ozone Symposium, Gottingen, A. Deepak Publishing, 1989.

Stachnik, R.A., J.C. Hardy, J.A. Tarsala, J.W. Waters and N.R. Erickson, Submillimeterwave heterodyne measurements of stratospheric ClO, HCl, O_3 and HO_2; first results, *Geophys. Res. Lett. 19*, 1931-1934, 1992

Swinbank, R. and A. O'Neill, A stratosphere-troposphere data assimilation system, *Mon. Wea. Rev.*, *122*, 686-702, 1994.

Toumi, R. and S. Bekki, The importance of the reactions between OH and ClO for stratospheric ozone, *Geophys. Res. Lett.*, *20*, 2447-2450, 1993.

Waters, J.W., et al Validation of UARS MLS ClO measurements, *J. Geophys. Res.*, **100**, (in press), 1995.

Weaver, C.J., A.R. Douglass and R.B. Rood, Thermodynamic balance of three-dimensional stratospheric winds derived from a data assimilation procedure, *J. Atmos. Sci.*, *50*, **2087-2993,** 1993.

Webster, C.R. et al. Chlorine chemistry on polar stratospheric cloud particles in the Arctic winter, *Science 261*, 1130-1134, 1993.

Woodbridge, E.L., et al., Estimates of total organic and inorganic chlorine in the lower stratosphere from in situ and flask measurements during AASE 11, *J. Geophys Res. 100*, 3057-3064, 1995.

Table 1. Chemical Species Contained in the Model

Transported	
O_x (= O_3 + $O(^3P)$ + **()('1)))**, H_2O_2	
NO_y (= NO + NO_2 + NO_3), N_2O_5, HNO_3, HO_2NO_2,	
ClO_y (= Cl + **('1o** + $2Cl_2O_2$), $ClONO_2$, HCl, HOCl, OClO,	
BrO_y (= Br + BrO), $BrONO_2$, BrCl, HBr, HOBr	
N_2O, CH_4, CO H_2O	

Table 2. Summary of SLIMCAT Model Experiments

This preprint was prepared with the AGU LaTeX macros v3.1. File ctm formatted 1996 April 29.

Run	Vertical Transport	J_{Cl2O2} Factor	Quantum Yield (R1)	(R3)
A	yes	1	0	0
B	no	1	0	0
C	no	1.5	0	0
D	no	1	0.08	0
E	no	1	0	0.003
F	no	1	0	0.03

Figure 1. Estimate of NO_y^* obtained from correlations with CLAES N_2O data using equation (1) for a) 465 K and b) 585 K on August 31 1992.

Figure 2. Sum of MLS HNO_3 and CLAES $ClONO_2$ and NO_2 (ppbv) for a) 465 K and b) 585 K on August 31 1992.

Figure 3. Position of the polar vortex (based on PV calculations) showing the inner vortex (dark shading) and the vortex edge (lighter shading) for a) 585 K September 5, b) 465 K September 5, c) 585 K September 15 and d) 465 K September 15.

Figure 4. Vortex averages of model ClO, ClO_x, HOCl, $ClONO_2$, HCl and Cl_y (ppbv) sampled at 1200 UT versus day (after August 31 1992) from run B for a) 585 K edge vortex, b) 585 K inner vortex, c) 465 K edge vortex and d) 465 K inner vortex.

Figure 5. Vortex averages of ascending MLS ClO (ppbv) and model ClO (ppbv) for a) 585 K vortex edge, b) 585 K inner vortex, c) 465 K vortex edge and d) 465 K inner vortex. The model has been sampled at the same local time as the MLS measurements for each grid point. The 465 K run B has also been sampled at 1200 local time at all longitudes. In addition results from run C are shown at 465 K and results from run D at 465 K and 585 K (sampled like MLS).

Figure 6. Vortex averages of ascending CLAES $ClONO_2$ (asterisks) and *model* $ClONO_2$ (ppbv) from run B and run D for a) 585 K vortex edge, b) 585 K inner vortex, c) 465 K vortex edge, and d) 465 K inner vortex. At 585 K the model $ClONO_2$ has been sampled at both 1200 UT and at the local time of the CLAES measurements. At 465 K the diurnal variation of $ClONO_2$ is *negligible* and the model is only sampled at 1200 UT. Note there is no CLAES data for September 1.

Figure 7. As figure 4 but for run D. Also shown as the vortex-averaged HCl from HALOE (+ marks).

Figure 8. As figure 4 but for run F.

Figure 9. HALOE observations of HCl (ppbv) interpolated to a) 585 K and b) 465 K. There are around 15 observations per day which progress southwards with time; the low latitude observations were made on September 12 and the highest latitude ones on October 5. Results from model run D (sampled at the same time and location as the HALOE observations) from September 15 to October 2 are shown in figures 8c and 8d.

Figure 10. Distribution of $ClONO_2$ from CLAES and model run D (sampled at the same local time as CLAES) for a) 585 K September 5, b) 465 K September 5, c) 585 K September 15 and d) 465 K September 15. The model fields are discontinuous at 180°E due to the 24 hour shift in UT across the date line. Bad data points have been removed from the CLAES maps and show up as areas of zeros, e.g. near the Palmer peninsula in figure 9a.

Figure 11. Distribution of ClO from MLS and model run D (sampled at the same local time as MLS) for a) 585 K September 5, b) 465 K September 5, c) 585 K September 15 and d) 465 K September 15. The model fields are discontinuous at 180°E due to the 24 hour shift in UT across the date line.

Figure 12. Vortex averages of MLS O_3 (triangles) and model O_3 (ppmv) from runs A,B,C and D for a) 585 K vortex edge, b) 585 K inner vortex, c) 465 K vortex edge and d) 465 K inner vortex.

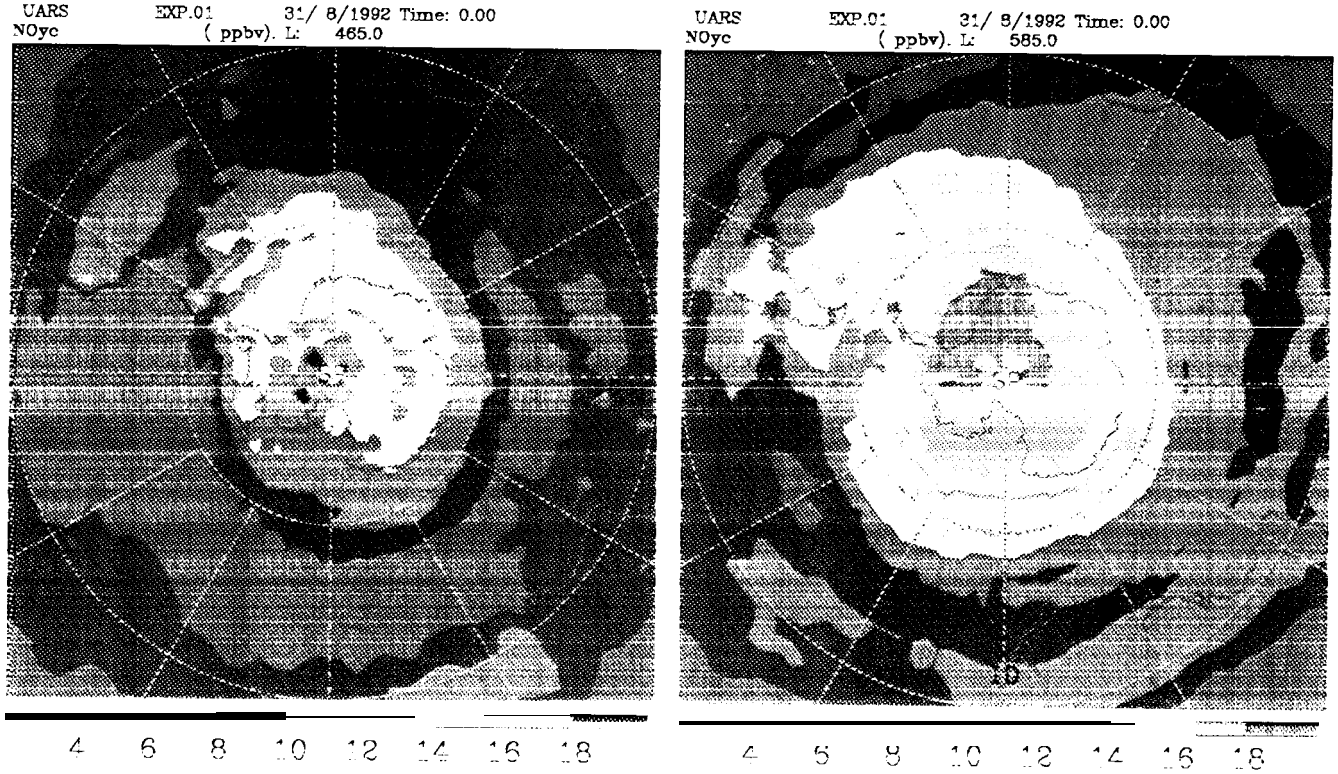
UARS
NOyc
EXP.01
31/ 8/1992 Time: 0.00
(ppbv). L: 465.0
4 6 8 10 12 14 16 18
UARS
NOyc
EXP.01
31/ 8/1992 Time: 0.00
(ppbv). L: 585.0
4 6 8 10 12 14 16 18

Figure 1

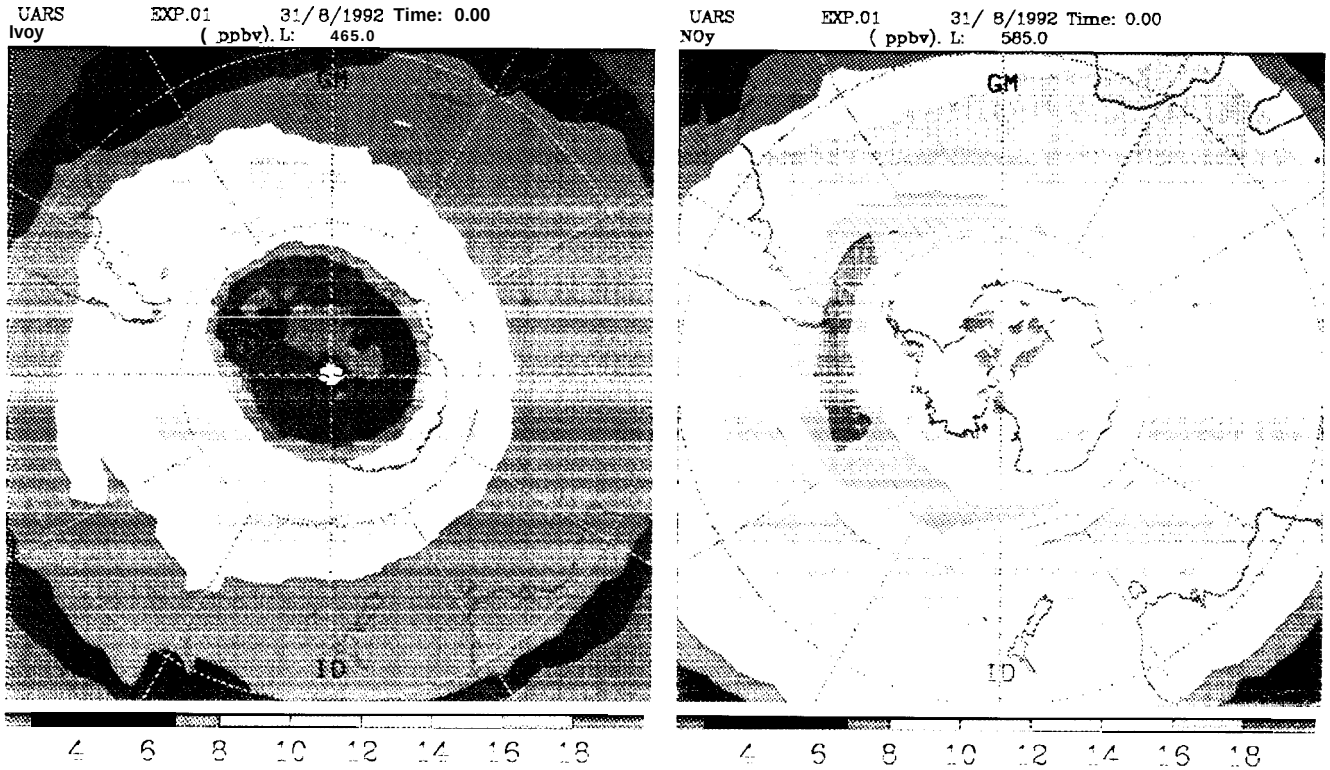
UARS EXP.01 31/ 8/1992 Time: 0.00
Ivoy (ppbv). L: 465.0
GM
ID
4 6 8 10 12 14 16 18
UARS EXP.01 31/ 8/1992 Time: 0.00
NOy (ppbv). L: 585.0
GM
ID
4 6 8 10 12 14 16 18

Figure 2

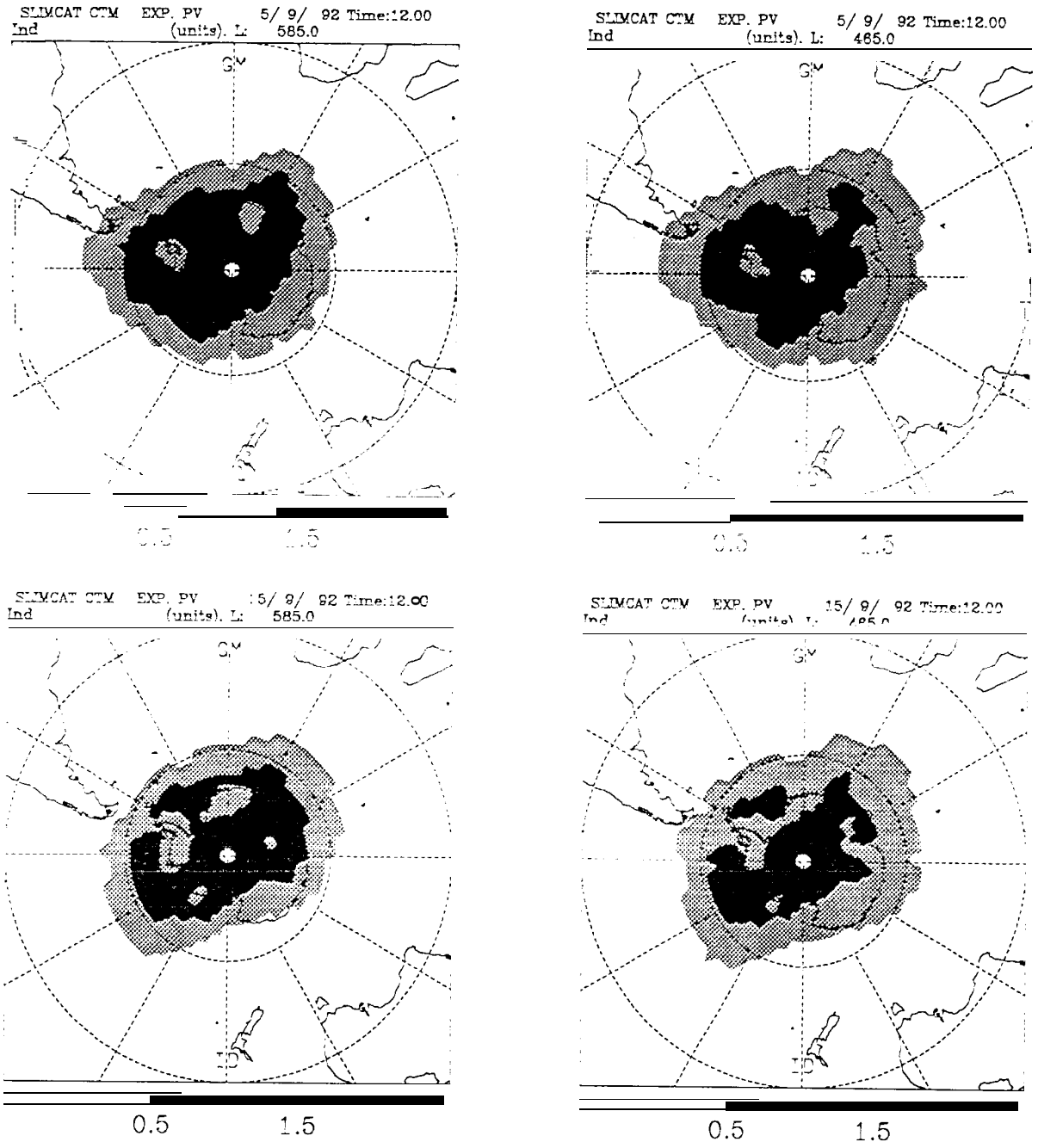
SLIMCAT CTM EXP. PV 5/ 9/ 92 Time:12.00
Ind (units). L: 585.0
GM
0.5
1.5
SLIMCAT CTM EXP. PV 5/ 9/ 92 Time:12.00
Ind (units). L: 485.0
GM
0.5
1.5
SLIMCAT CTM EXP. PV 5/ 9/ 92 Time:12.00
Ind (units). L: 585.0
GM
0.5
1.5
SLIMCAT CTM EXP. PV 15/ 9/ 92 Time:12.00
GM
0.5
1.5

Figure 3

585K edge

585K inner

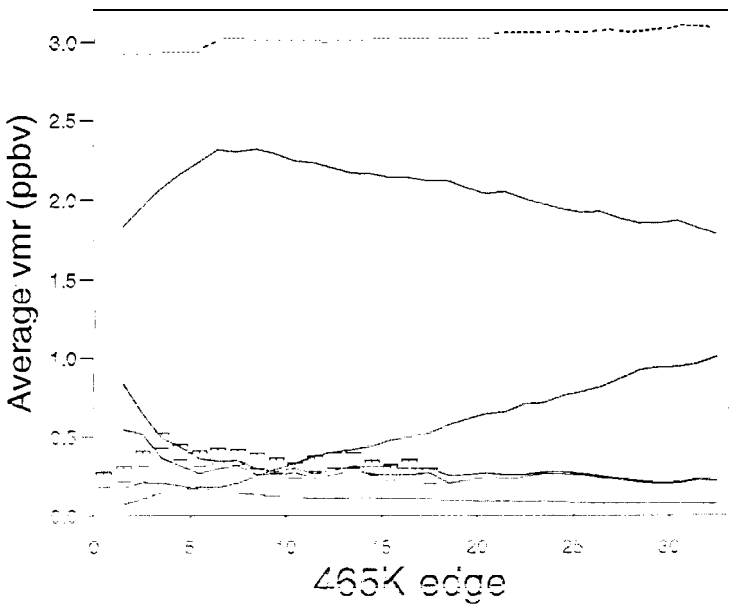

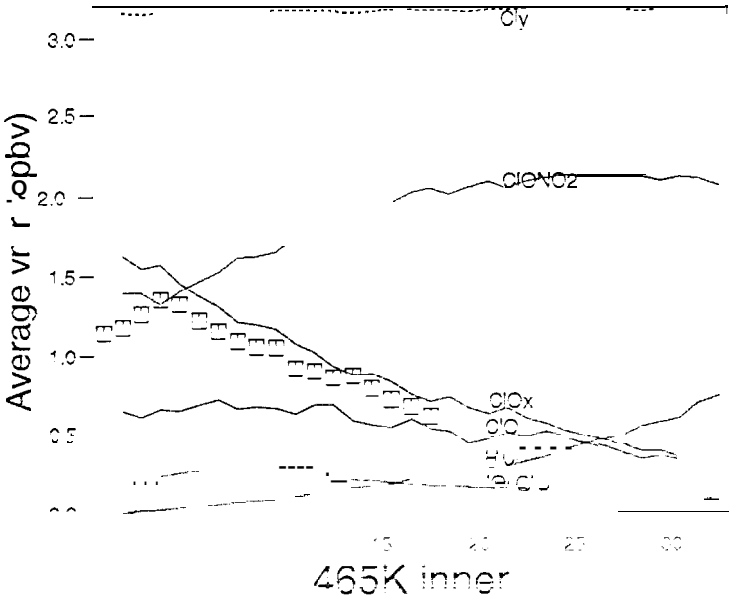

465K edge

465K inner

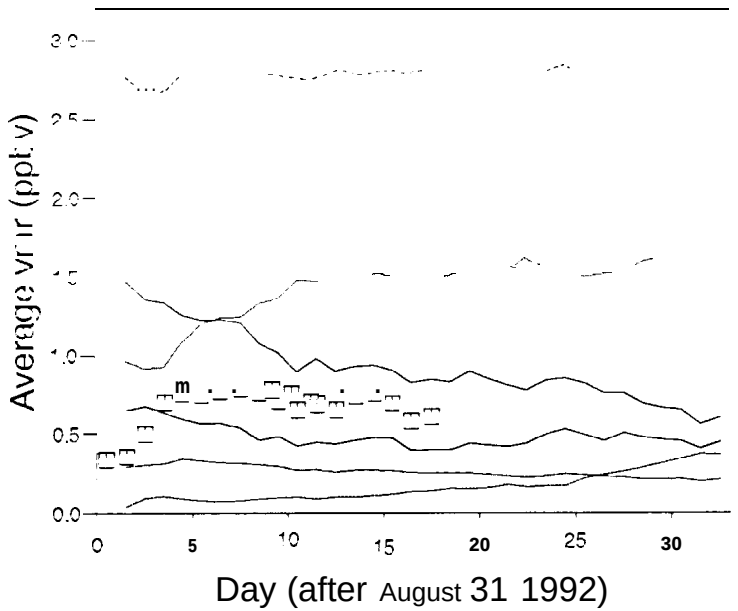

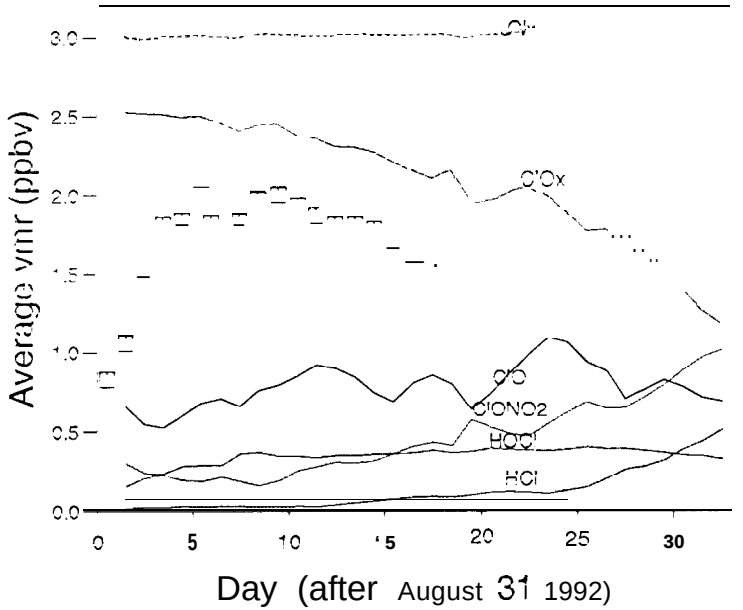

Figure 15

585K edge

585K inner

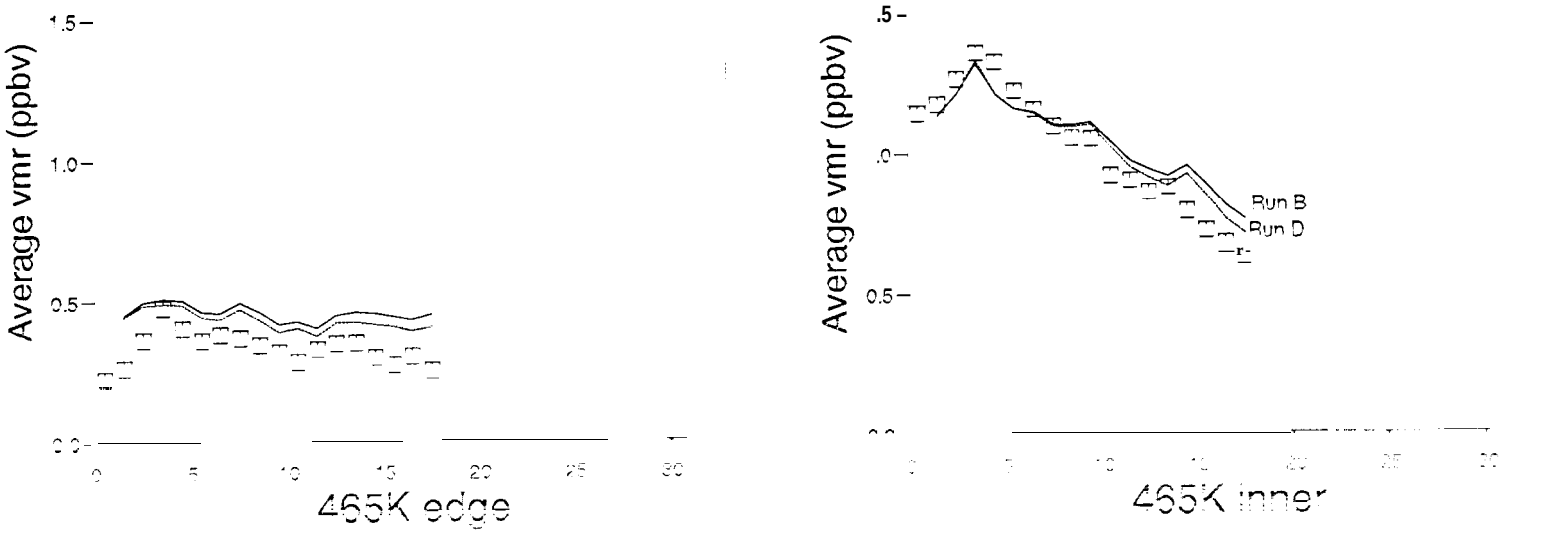

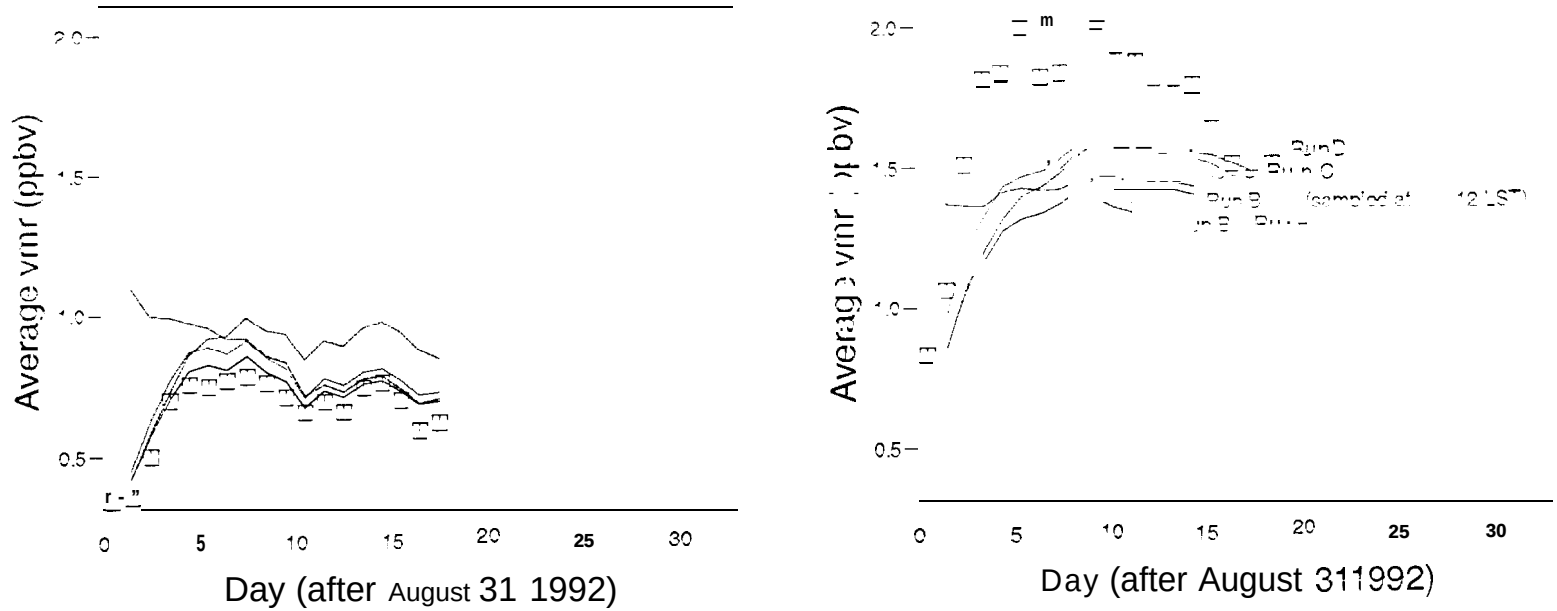

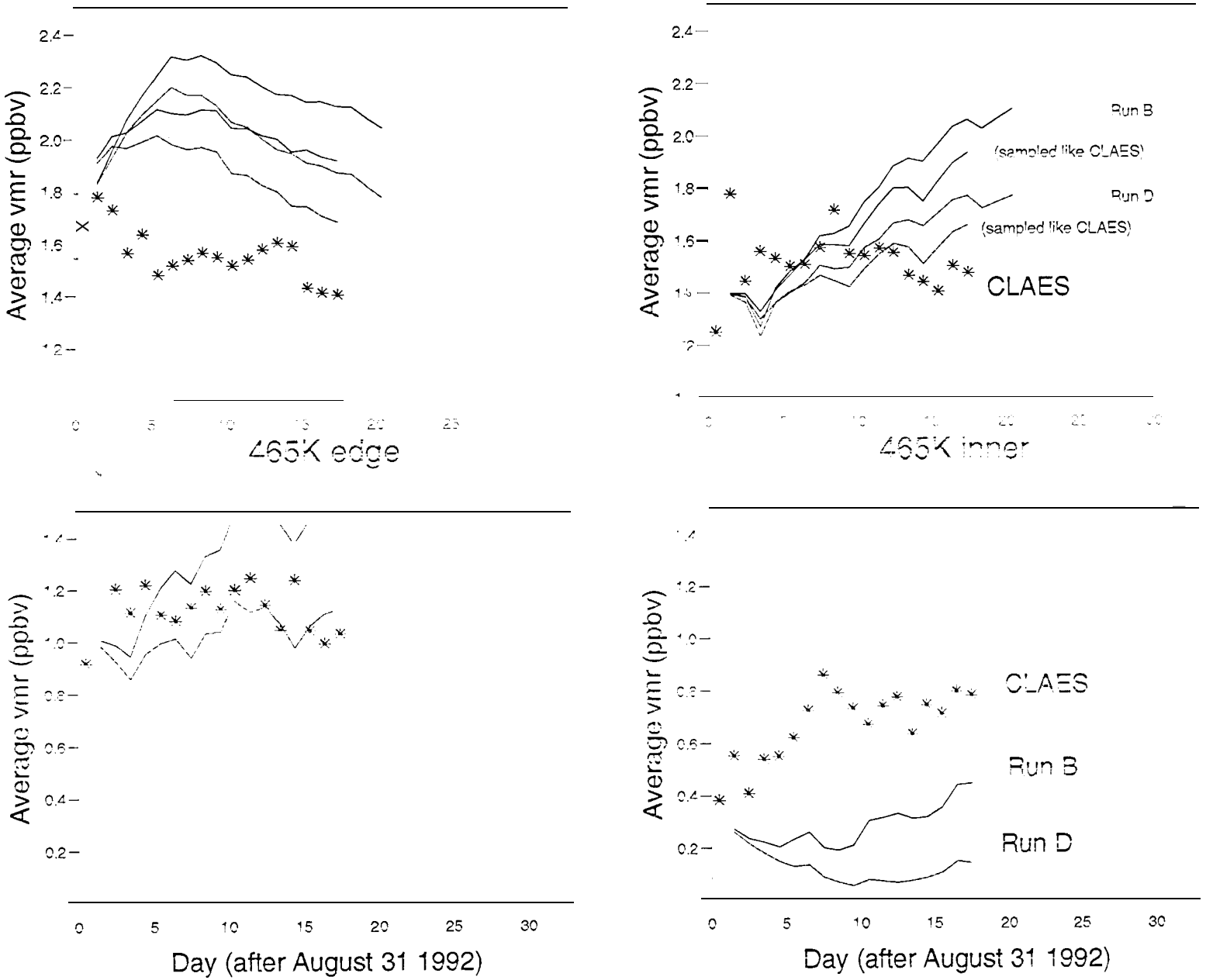
585K edge
585K inner
Average vmr (ppbv)
Run B
(sampled like CLAES)
Run D
(sampled like CLAES)
CLAES
465K edge
465K inner
Average vmr (ppbv)
CLAES
Run B
Run D
Day (after August 31 1992)
Day (after August 31 1992)

Figure 6

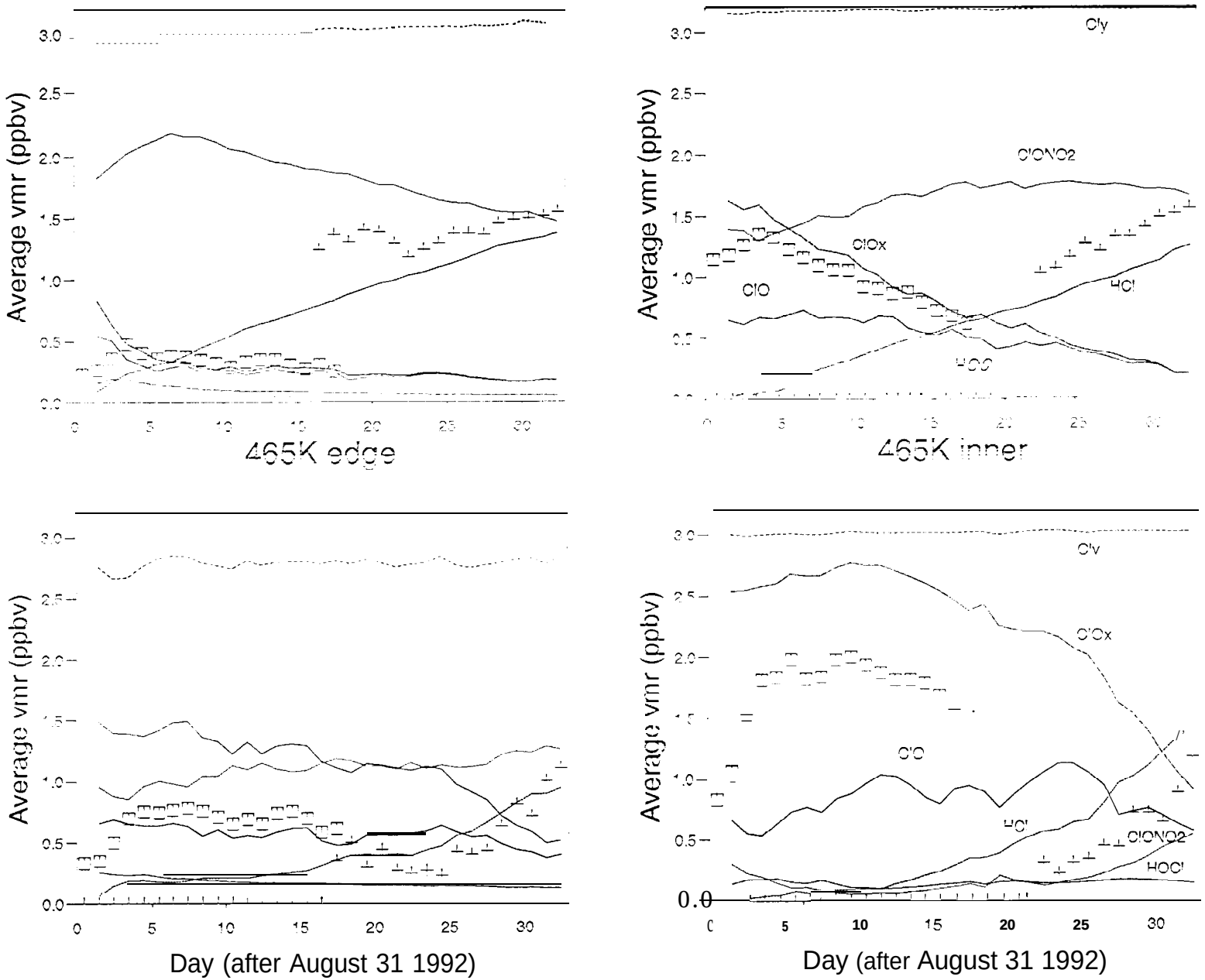
585K edge
585K inner
Cly
ClONO2
ClOx
ClO
HCl
HOCl
465K edge
465K inner
Average vmr (ppbv)
Day (after August 31 1992)

Figure 7

Figure 9a

HALOE data 585 K

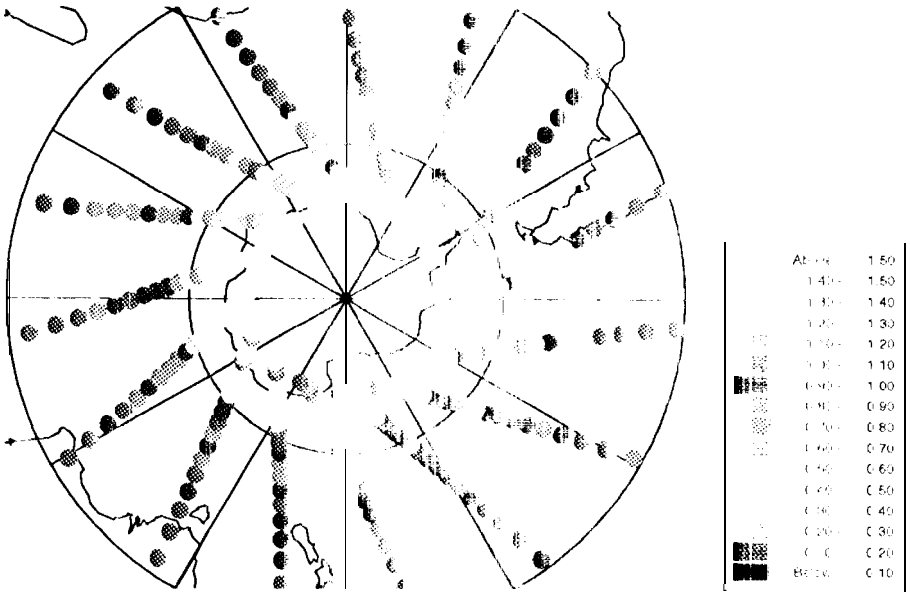

Figure 9b

HALOE data 465 K

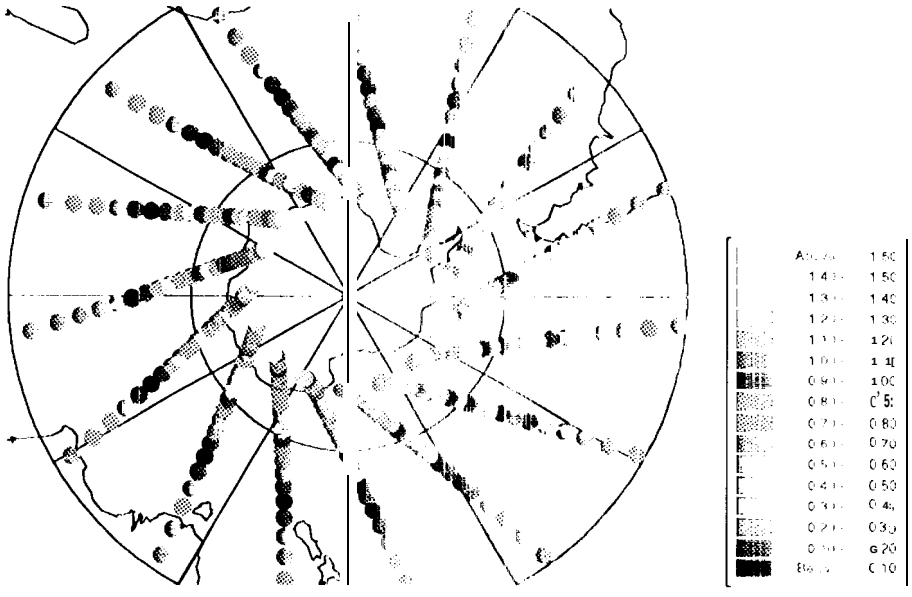

Figure 9c

CTM HCL expD 585 K

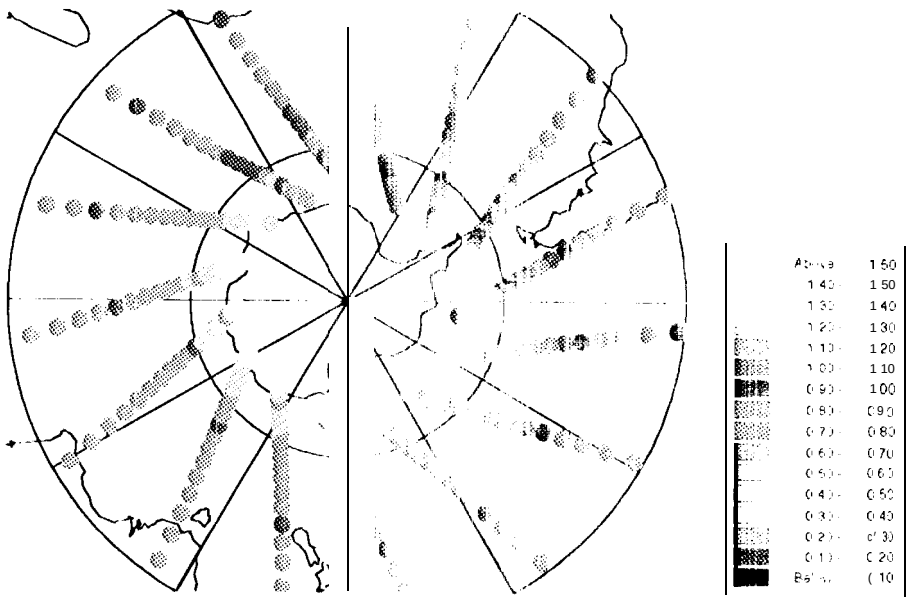

Figure 7d

CTM HCL exp D 465 K

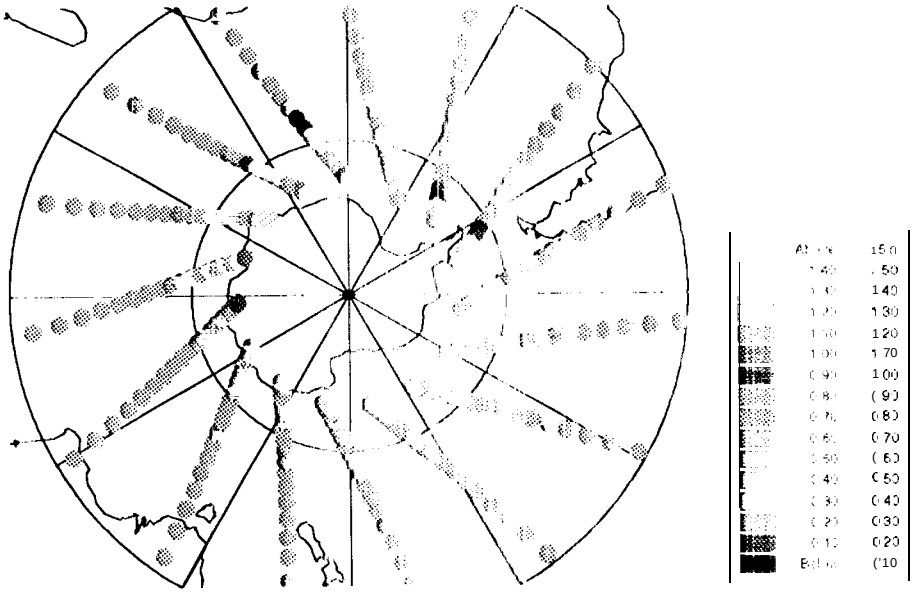

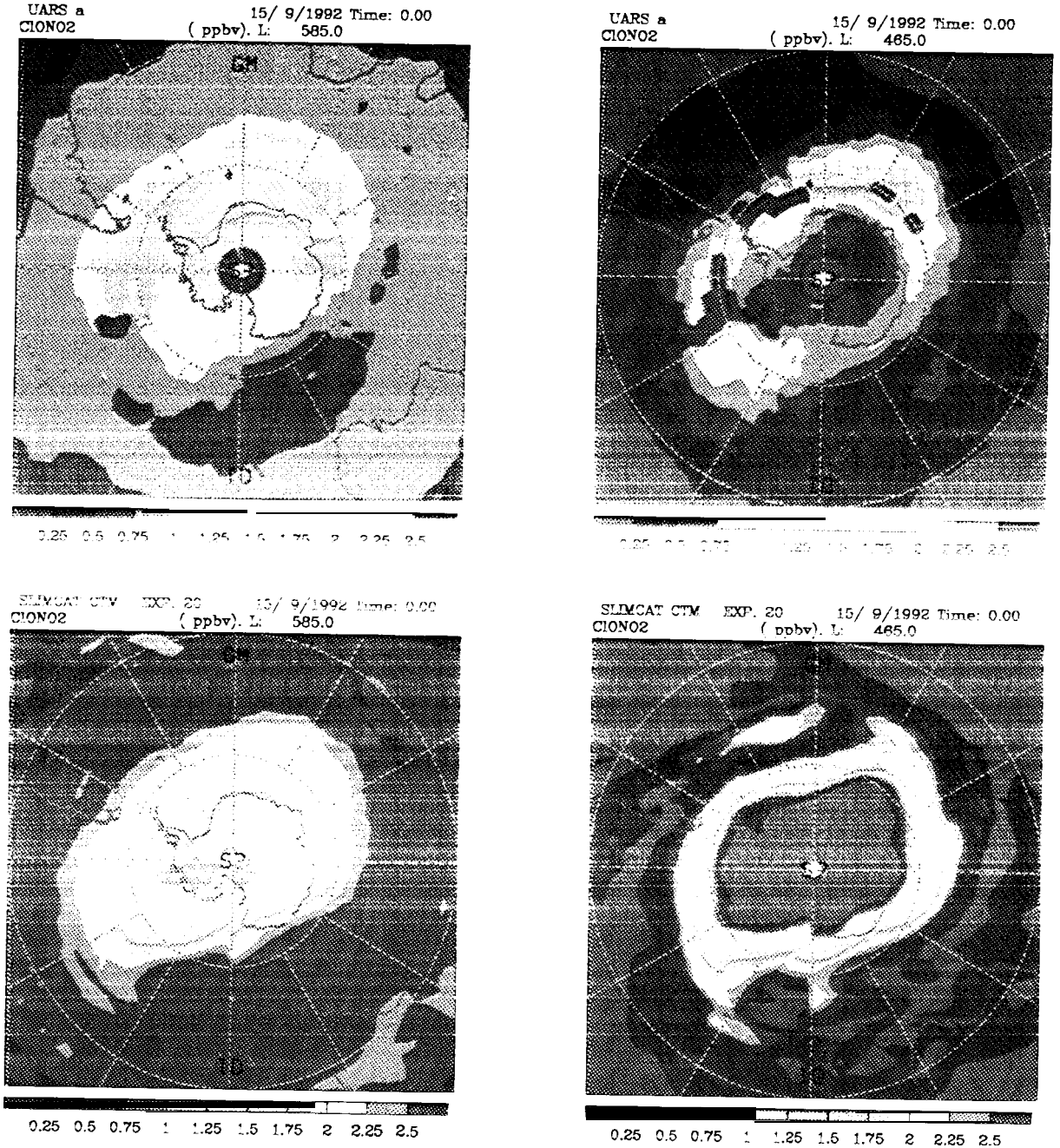
UARS a
ClONO2
15/ 9/1992 Time: 0.00
(ppbv). L: 585.0
UARS a
ClONO2
15/ 9/1992 Time: 0.00
(ppbv). L: 465.0
SLIMCAT CTM EXP. 20
ClONO2
15/ 9/1992 Time: 0.00
(ppbv). L: 585.0
SLIMCAT CTM EXP. 20
ClONO2
15/ 9/1992 Time: 0.00
(ppbv). L: 465.0
0.25 0.5 0.75 1 1.25 1.5 1.75 2 2.25 2.5
0.25 0.5 0.75 1 1.25 1.5 1.75 2 2.25 2.5

Figure 10 a/b

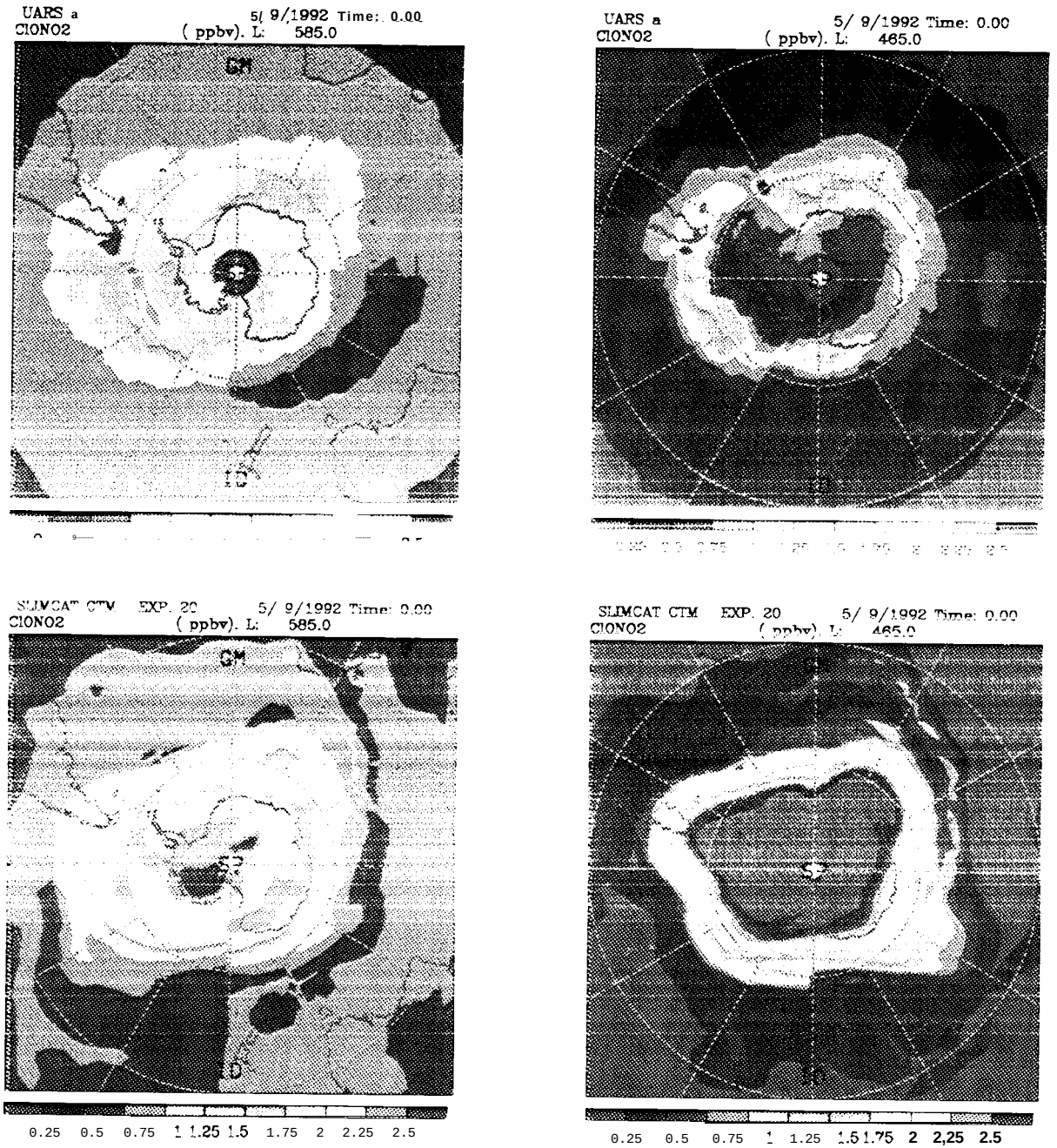
UARS a
ClONO2
5/ 9/1992 Time: 0.00
(ppbv). L: 585.0
UARS a
ClONO2
5/ 9/1992 Time: 0.00
(ppbv). L: 465.0
SLIMCAT CTM EXP. 20
ClONO2
5/ 9/1992 Time: 0.00
(ppbv). L: 585.0
SLIMCAT CTM EXP. 20
ClONO2
5/ 9/1992 Time: 0.00
(ppbv). L: 465.0
0.25 0.5 0.75 1 1.25 1.5 1.75 2 2.25 2.5
0.25 0.5 0.75 1 1.25 1.5 1.75 2 2,25 2.5

Figure 10 cd.

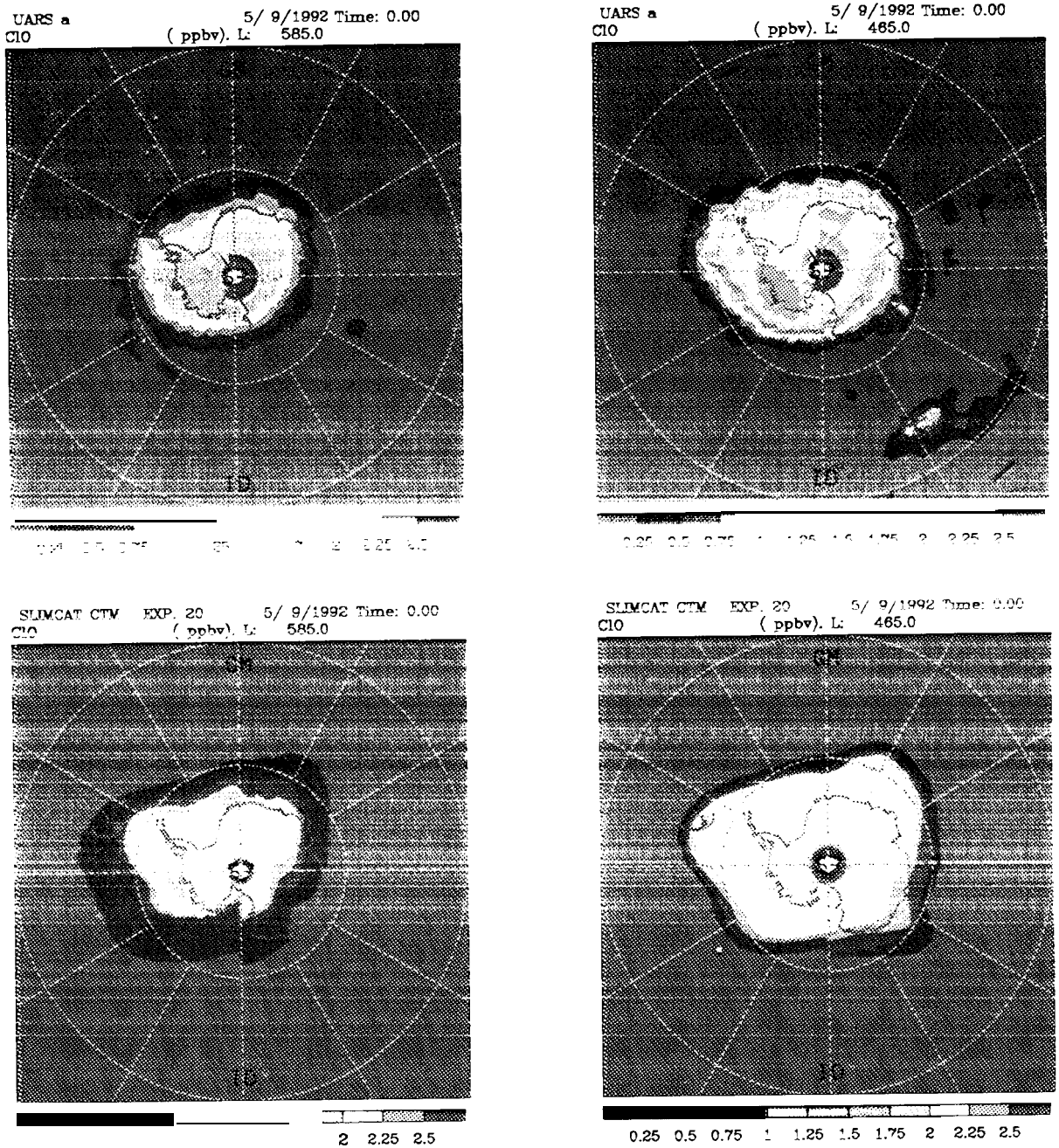
UARS a
5/ 9/1992 Time: 0.00
ClO
(ppbv). L: 585.0
UARS a
5/ 9/1992 Time: 0.00
ClO
(ppbv). L: 465.0
SLIMCAT CTM EXP. 20
5/ 9/1992 Time: 0.00
ClO
(ppbv). L: 585.0
SLIMCAT CTM EXP. 20
5/ 9/1992 Time: 0.00
ClO
(ppbv). L: 465.0
2 2.25 2.5
0.25 0.5 0.75 1 1.25 1.5 1.75 2 2.25 2.5

Figure 4.a.b

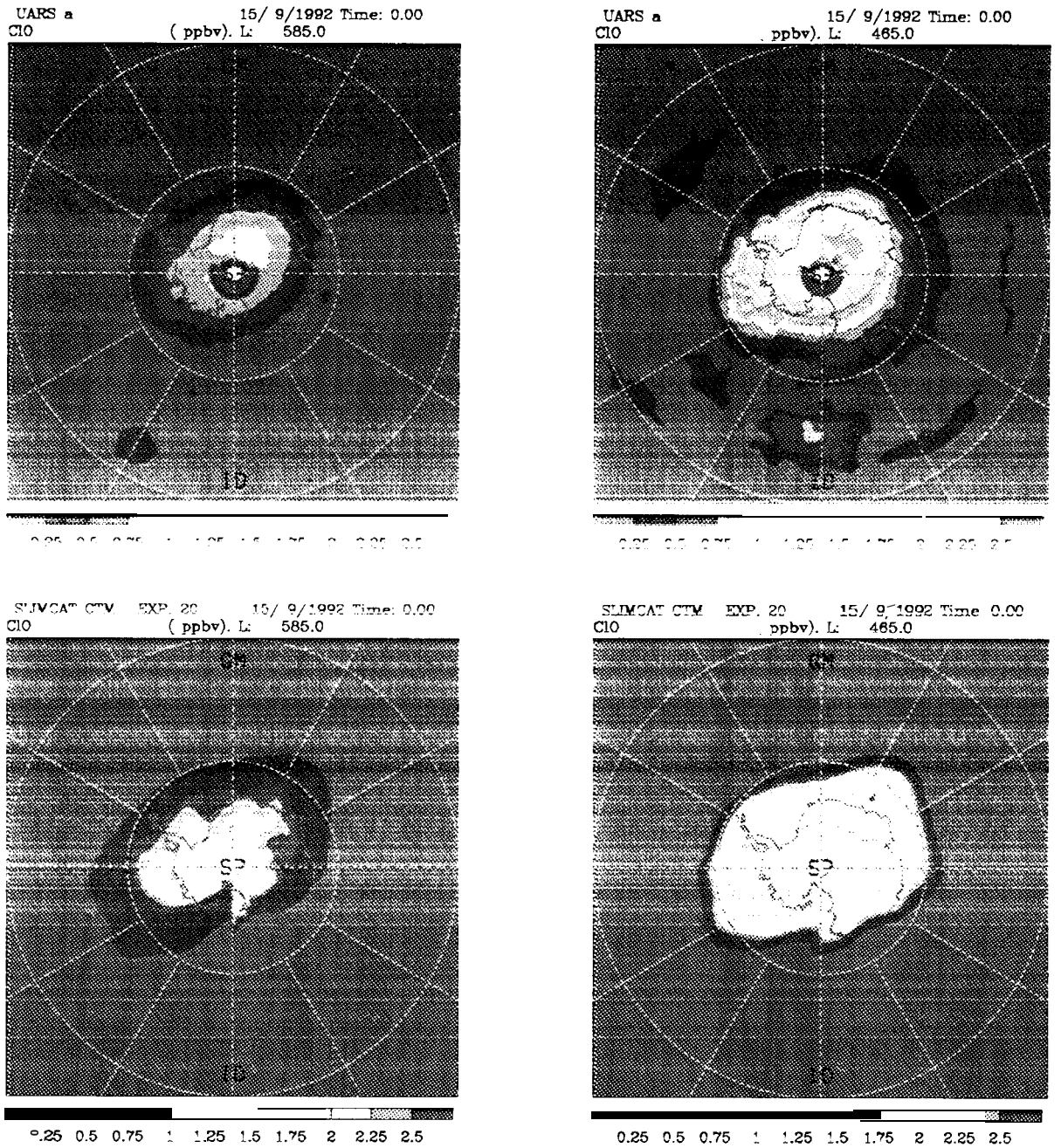
UARS a
15/ 9/1992 Time: 0.00
ClO
(ppbv). L: 585.0
UARS a
15/ 9/1992 Time: 0.00
ClO
ppbv). L: 465.0
SLIMCAT CTM EXP. 20
15/ 9/1992 Time: 0.00
ClO
(ppbv). L: 585.0
SLIMCAT CTM EXP. 20
15/ 9/1992 Time 0.00
ClO
ppbv). L: 465.0
0.25 0.5 0.75 1 1.25 1.5 1.75 2 2.25 2.5
0.25 0.5 0.75 1 1.25 1.5 1.75 2 2.25 2.5

Figure 1: cd

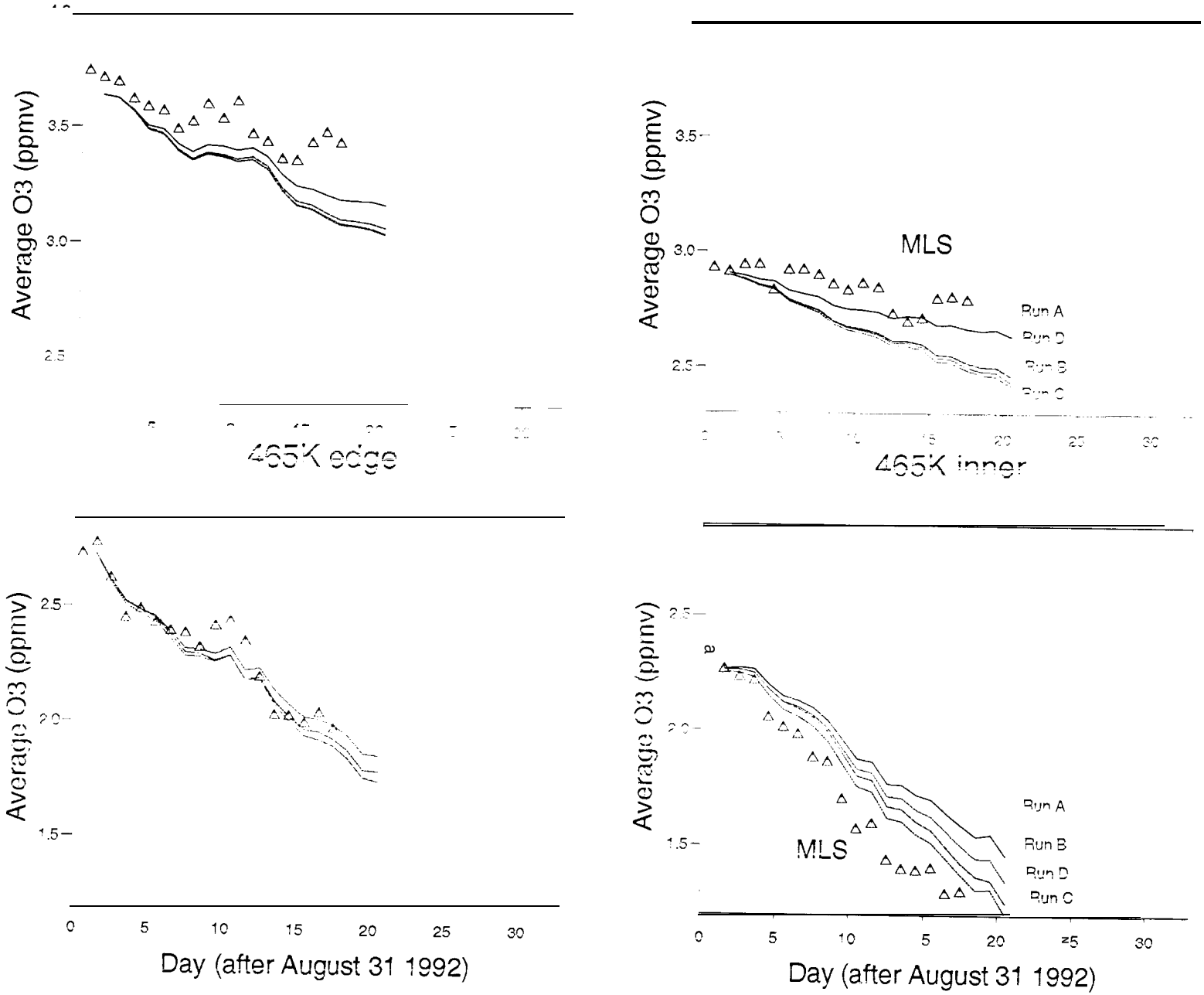
585K edge
585K inner
Average O3 (ppmv)
3.5
3.0
2.5
MLS
Run A
Run D
Run B
Run C
465K edge
465K inner
2.5
2.0
1.5
0
5
10
15
20
25
30
Day (after August 31 1992)

Figure 12